ELSEVIER

Contents lists available at ScienceDirect

Climate Services

journal homepage: www.elsevier.com/locate/cliser



Original research article

High time- and spatial-resolution climate scenarios of the DISTENDER project according to statistical and dynamical downscaling

Robert Monjo ^{a,b,*}, Yassmin H. Essa ^{c,d}, Carlos Prado-López ^b, Manpreet Kaur ^{c,e}, Darío Redolat ^b, César Paradinas ^b, Dominic Royé ^f, Bodo Ahrens ^c, Roberto San José ^g

- ^a Area of Physics and Mathematics, Alfonso X El Sabio University Madrid Campus Chamberf. C/ Arapiles, 13, E- 28015, Madrid, Spain
- ^b Climate Research Foundation Fundación para la Investigación del Clima (FIC), Madrid, Spain
- ^c GUF-IAU Goethe University Frankfurt, Institute for Atmospheric and Environmental Sciences (GUF-IAU), Frankfurt am Main, Germany
- ^d Agricultural Research Center, Central Laboratory for Agricultural Climate (ARC-CLAC), Giza, Egypt
- e The Nature Conservancy, Arlington, USA
- f Misión Biologica de Galicia The Spanish National Research Council (CSIC), Spain
- g Universidad Politécnica de Madrid (UPM), Madrid, Spain

ARTICLE INFO

Keywords: Statistical downscaling Dynamical downscaling Climate modeling Climate hazards

ABSTRACT

This paper discusses statistical and dynamical methods used to produce local (grid-spacing < 4 km) and European (~10 km) climate scenarios that were used as input for multi-sectoral impact models in the DevelopIng STratEgies by integrating mitigatioN, aDaptation and participation to climate changE Risks (DISTENDER) project, and shares the main results with a special focus on temperature and precipitation. The statistical downscaling consisted of three stages: (1) a parametric quantile mapping at a daily scale; (2) an analogoustransference function of hourly curves for each day, and (3) a classical geostatistical downscaling. This threestage technique was applied to three representative Earth System Models according to three different climatechange level (being EC-EARTH3-Veg the medium case) under four shared socioeconomic pathways (SSP1-2.6, SSP2-4.5, SSP3-7.0, SSP5-8.5). In addition, dynamical downscaling was also considered. Particularly, the ICOsahedral Nonhydrostatic model downscaled the EC-EARTH3-Veg model to computationally costly km-scale resolution under all four pathways. Both downscaling approaches show consistent behaviour for the downscaled model under the different pathways. Results indicate historical biases in precipitation about \pm 10 % in general, while temperature biases ranged from $-2^{\circ}\mathrm{C}$ to $+1^{\circ}\mathrm{C}$ across different regions and seasons. Under SSP5-8.5, summer precipitation in southern Europe is projected to decrease by up to 20 %, while northern Europe experiences increases of + 10 % to + 15 %. Temperature increases under the same scenario reach + 5°C in summer across southern Europe, with smaller increases of $+2^{\circ}$ C to $+3^{\circ}$ C in northern regions. These findings on management for uncertainty levels demonstrate the utility of combined downscaling approaches for local climate risk assessment and adaptation strategies.

Practical implications

The DISTENDER project provides high-resolution climate scenarios that can directly support policy makers, urban planners, and climate adaptation practitioners in developing informed strategies for mitigating climate risks (https://distender.eu/). By integrating statistical and dynamical downscaling approaches, DISTENDER offers climate projections at both local (<4 km) and

European (~10 km) scales, ensuring more precise climate information tailored to specific regions and decision-making needs.

One of the primary applications of DISTENDER's climate projections is in climate risk assessment for urban areas, agricultural regions, and coastal communities. For instance, in Southern Europe, where summer precipitation is projected to decrease by up to 20 % under the SSP5-8.5 scenario, water management authorities can use these projections to optimize reservoir operations, promote water-saving technologies, and implement drought mitigation measures. Similarly, Northern Europe's projected

^{*} Corresponding author at: Area of Physics and Mathematics, Alfonso X El Sabio University - Madrid Campus Chamberí, C/ Arapiles, 13, E- 28015, Madrid, Spain. E-mail address: rmonjagu@uax.es (R. Monjo).

precipitation increases (+10 % to +15 %) can help urban planners reinforce drainage systems to prevent flooding and infrastructure damage.

The integration of hourly-scale projections is particularly useful for extreme event preparedness, such as to face heatwaves. For example, under the same SSP5-8.5 scenario, temperature increases of up to 5 $^{\circ}$ C in summer necessitate adaptive strategies, such as modifying building designs to improve thermal insulation, increasing green urban spaces, and implementing early warning systems to protect vulnerable populations from extreme heat events.

Sectoral applications of the downscaled climate data include agriculture and water resource management. In areas where drought risk is expected to intensify, such as Southern Spain and Italy, farmers can transition to drought-resistant crops, adopt precision irrigation techniques, and implement soil moisture conservation practices. In contrast, increased rainfall in Central and Northern Europe may require modifications in crop selection and irrigation scheduling to avoid waterlogging and soil degradation. Concerning urban planning, cities and municipalities can leverage DISTENDER's projections to enhance climate resilience in infrastructure development. For example, in regions facing increased storm intensity and higher rainfall variability, stormwater management plans should incorporate permeable pavements, rain gardens, and improved flood defenses. Heatwave projections can inform cooling strategies, including increased tree cover, cool roofing technologies, and the design of urban spaces to mitigate the urban heat island effect.

Climate variability significantly impacts renewable energy production, particularly wind and solar power. By using DISTENDER's projections of wind variability and solar radiation trends, energy grid operators and planners can optimize the placement of wind turbines and solar farms. For instance, projected shifts in wind patterns in Northern Europe can influence offshore wind farm efficiency, while solar energy production in Southern Europe may benefit from reduced cloud cover.

The availability of high-resolution hourly climate data provides valuable input for governmental and institutional decision-making processes. Climate-sensitive sectors, such as public health and disaster management, can use this data to refine heatwave action plans and emergency response strategies. The probabilistic nature of the downscaled projections allows for more accurate risk assessments, helping policymakers prioritize adaptation investments based on multiple climate change scenarios. Furthermore, the European Union's Green Deal and national adaptation frameworks can integrate DISTENDER's projections to set more precise climate goals. For example, policymakers aiming to achieve net-zero emissions can use localized temperature projections to assess the potential for urban heat stress reduction via green infrastructure initiatives.

To demonstrate the practical application of DISTENDER's projections, a case study was conducted in the Metropolitan City of Turin (CMTo), an urban area with complex topographical and climatic conditions. Using statistical downscaling, high-resolution temperature and precipitation projections were generated, allowing city planners to assess climate risks at the neighborhood level. The key findings are: i) Under SSP5-8.5, CMTo is expected to experience temperature increases of up to 4 °C by 2050, with the most significant warming during summer; ii) projected precipitation trends indicate a decrease in overall rainfall but an increase in extreme precipitation events, elevating the risk of flash floods; iii) the urban heat island effect is likely to intensify, requiring additional cooling interventions, such as expanded tree planting and reflective surface materials in urban design. Based on these projections, CMTo's adaptation plan now includes revised heat emergency protocols, climate-resilient infrastructure investments, and a focus on enhancing public awareness of climate risks.

To maximize the utility of DISTENDER's climate projections, stakeholders should consider the following implementation

strategies: a) Incorporate climate projections into land-use planning, zoning regulations, and disaster preparedness programs in local government and municipalities; b) enable water management authorities to develop integrated water resource management plans using projected precipitation variability data; support urban planners and architects in designing climate-adaptive infrastructure and buildings to withstand future climatic conditions; c) training energy sector technicians to utilize wind and solar projections to optimize renewable energy investments; d) supporting agricultural policy makers in adjusting policies to encourage climate-smart agricultural practices and sustainable water use.

Therefore, the DISTENDER project bridges the gap between global climate modeling and localized adaptation needs, providing actionable climate intelligence for multiple sectors. By integrating these high-resolution projections into decision-making frameworks, stakeholders can enhance resilience against climate change impacts and develop sustainable adaptation strategies tailored to specific regional challenges. As climate conditions continue to evolve, continued refinement and expansion of downscaling methodologies will further improve the accuracy and applicability of climate services, reinforcing the ability of societies to mitigate and adapt to climate risks effectively.

1. Introduction

One of the main obstacles when studying climate-related risks is that Earth System Models (ESM) have a coarse-resolution grid which is unable to capture local phenomena playing a very important role in the regional climatic conditions, particularly for the occurrence of natural hazards and their impacts. For these reasons, it is essential that future climate projections take better into account the peculiarities of each area in order to understand future climate-related risk more reliably.

In 1996 World Climate Research Programme (WCRP) initiated a project to assess and compare global coupled climate model experiments, popularly known as Coupled Model Intercomparison Project (CMIP). The project completed five phases until 2014, with tremendous success in providing multi-model output to climate researchers and users internationally. It has thus turned out to be a cornerstone of global climate change evaluations.

The successor phase six (CMIP6) of the project began in 2016 to sustain the progress made in understanding climate change and associated evolution with updated climate models. CMIP6 is visioned to support WCRP grand science challenges by focusing on three key scientific questions: 1) What is the earth system's response to forcing? 2)What are the sources of systematic climate model biases and their impact? 3) How can future changes in the earth's climate be assessed involving intricate internal variability and predictability?

These objectives are elaborated through 21 sub-projects known as MIPs, for example, aerosol chemistry, carbon cycles, radiative forcing, volcanic eruptions, ocean, land surface, ice sheets, monsoons, paleoclimate, geoengineering, and so forth. CMIP6 was planned initially to incorporate runs from 100 climate models generated at 49 modelling groups, and as of 2020, results from nearly 40 models have been published, highlighting significant improvements over phase five models. The historical simulations are available for 1850–2014, whereas future projections are from 2014 onwards. However, Climate scientists can use a few initial years of projection simulations for present-day climate assessment where historical runs are closely connected to future projections (Eyring et al., 2016).

The future projections are based on the new shared socioeconomic pathways (SSPs) framework given by the energy modelling community in contribution to IPCC AR6. Ih this, an integrated approach is attempted to produce scenarios from the combination of existing representative concentration pathways for climate projections, socioeconomic considerations, and climate policies. CMIP6 selects a number of SSPs for

climate model run distributed among two tiers. In particular, Tier 1 was selected in this study because it corresponds to the core experimental set of the IPCC AR6, consisting of four socioeconomic pathways: SSP5-8.5, SSP3-7.0, SSP2-4.5, and SSP1-2.6 (Cos et al., 2022).

Further, to provide adequate climate information at a local scale, it is necessary to apply a suitable downscaling process based on either statistical (from now on, SDS) or dynamical (from now on, DDS) approach on very high resolution (Ribalaygua et al., 2013, Monjo et al., 2016, IPCC, 2021). For instance, Med-CORDEX (Somot et al., 2018) provides downscaled CMIP5 and CMIP6 climate scenarios with 12 km gridspacing. This is still coarse to the grid-spacing of 3 km and better targeted in the project DevelopIng STratEgies by integrating mitigatioN, aDaptation and participation to climate changE Risks (DISTENDER) project (San Jose et al., 2024). Available km-scale DDS products as produced in, for example, Copolla et al. (2020) or Ban et al. (2021) cover limited domains only because of computational costs. On the other hand, SDS efforts were performed in the Chelsa project (Brun et al., 2022) and Copernicus-C3S (2020, 2022). However, there exists some remarkable differences among the different approaches considered. For example, statistical approaches show two main disadvantages compared to DDS (Ribalaygua et al., 2013): (1) they have a strong dependency on historical observations and thus there may be a possible problem of nonstationarity in the relationships between predictors and predictands when weak physical linkages are used; (2) they can present spatial or inter-variable inconsistencies due to independent simulations for each variable and/or point.

On the other hand, the main advantages of the statistical approaches are four summarised in two points (Table 1). The first (A) is the low computational cost, which allows the downscaling of a large number of ESM outputs and greenhouse gas emission scenarios in order to quantify uncertainties, but more human resources are required. The second (B) is that specific information is provided for the same observed reference data (reanalysis grid point or observatories), and they provide more details on the probability distribution tails (extremes) and other microclimatic features. The local detail used in SDS is relevant as the same future climate may bring changes with respect to the current climate which could be quite different for points which are a few km apart.

DDS can be computationally expensive, but it is based on physical principles representing the actual atmospheric and climatic conditions and is more suitable for studying climate change than the statistical approaches relying on past climate relationships.

On the other hand, statistical approaches for observatories have the advantage of using real data to better simulate all probability distributions (including heavy-tailed ones). For the particular characteristics of

Table 1Summary of the main advantages/disadvantages of the SDS and DDS approaches and their secondary features linked.

Feature	SDS	DDS
(1) Historical observations of the studied variables are not needed	×	1
Stationary predictors/predictands relationships are guaranteed (from 1)	Sometimes	1
(2) Spatial and inter-variable consistency is guaranteed	×	1
No-predetermined experiments of climate sensitivity (from 2)	×	1
Few human resources required (from 2)	×	✓
Low computational cost / fast production of results	1	×
Large multi-method, multi-scenario & multi-model ensemble (from A)	1	×
Spatial resolution as fine as possible (e.g. for a station)	1	×
Products are mainly unbiased (from B)	/	×
Probability distribution with adequate extreme point values (from B)	1	Sometimes

the statistical approaches used in DISTENDER, the advantages are the following: (1) predictors selection is based on theoretical considerations, trying to reflect the physical linkages between predictors and predictands, which to some extent reduces the stationarity problem; (2) it operates at the maximum spatial and temporal resolution offered by ESMs; (3) it considers the full range of data variability; and (4) it performs linear analysis on the hourly basis of physical forcing from topographic and land-use features after an analogue stratification, which reduces the non-linearity of the relationships between predictors and predictands. However, similar to the choice of the specific dynamical downscaling model selected, there exists also an uncertainty source that is strictly related to the adopted statistical methodology and the calibration period used for training.

This paper is structured in three main sections: (2) Climate data sources, including the reference reanalysis and Earth System Models; (3) Downscaling techniques, where both statistical and dynamical approaches are described; and (4) Preliminary results to advance early results of both experiments.

2. Climate data

2.1. Reference climate data

For statistical downscaling, we collected reanalysis datasets from the European Centre for Medium-Range Weather Forecasts (ECMWF): ERA5 (atmospheric) and primarily ERA5-Land (surface), which were used as "observed references" to correct the probability distributions of the CMIP6 climate models (Sect. 3.1.3.1). These datasets were selected for several key reasons: 1) They provide data for all the climate variables required in the statistical downscaling; 2) As ECMWF products, they provide superior data quality compared to other reanalyses, especially within Europe; 3) They represent the latest global reanalysis versions, offering improved spatial and temporal resolution over previous iterations; 4) They are freely accessible via the Copernicus Climate Change Service. Although a Copernicus regional reanalysis for Europe (CERRA; Ridal et al., 2024) was available, it did not fully cover our initial modeling domain for progressive nested dynamical downscaling.

ERA5-Land is a surface-specific dataset, focused exclusively on terrestrial regions, with data available for up to 50 variables. It features a global grid with a native resolution of 9 km \times 9 km (Copernicus-C3S, 2024), regridded to an experimental resolution of $0.073^{\circ} \times 0.073^{\circ}$ (our selection) and a standard resolution of $0.1^{\circ} \times 0.1^{\circ}$. Its vertical coverage extends from 2 m above the surface down to a depth of 289 cm, structured into four levels corresponding to the ECMWF surface model. The dataset provides hourly data from January 1951 to the present, with monthly updates, though data availability typically lags by around three months.

ERA5, ECMWF's latest atmospheric reanalysis, has been available since July 2019 and is currently the most accurate atmospheric reanalysis dataset. It integrates a vast array of observational data, including weather station measurements, atmospheric soundings, satellite observations, and other reanalysis datasets (such as oceanic data), to reconstruct atmospheric and marine conditions at various levels. ERA5 aims to reproduce past atmospheric states as accurately as possible. Due to the high-quality data requirements, satellite-based information is only available post-release. The dataset covers all of Europe with a regular spatial resolution of 0.25° (approximately 30 km).

2.2. Climate models

Due to limited computational resources available for the sectoral modeling of DISTENDER (e.g. air pollution and human health; San Jose et al., 2024, Relvas et al., 2025), we needed to select three representative CMIP6 climate models from the starting point of ten CMIP6 climate models (with subdaily resolution), which were previously downscaled in the FIREURISK project for the whole European domain at a 0.073°

spatial resolution (Hetzer et al., 2024). These ten CMIP6 candidates were then sorted by "level of climate change" in temperature by 2050: (a) low-change level (25 %) corresponds to MPI-ESM1-2-HR; (b) medium-change level (50 %) is for EC-EARTH3-Veg; and (c) high-change level (75 %) is for the CanESM5 model (Table 2). For the adaptation measures, only the medium-change level simulation has been considered. Therefore, the main results of this study were focused on the model EC-EARTH3-Veg since it represents approximately the 50 % climate change level.

Consistently, taking into account the limitations posed by computational resources, only EC-EARTH3-Veg simulations were dynamically downscaled. The climate data from CMIP6 models is collected and archived at Earth System Grid Federation (ESGF) data replication centers and Copernicus. In DDS, the global historical climate simulation and future projections were downscaled over the Med-CORDEX domain in DDS, and over a grid covering Europe (between latitudes 29°N and 56°N and longitudes between 12°W and 43°E) for SDS.

DISTENDER defined 14 domains to model climate variables in the five Core Case Studies. For operational reasons, only 11 domain areas were finally selected from these to produce both hourly and daily climate scenarios, while the three other (larger) domains were just for daily products (Appendix A, Table A1). The total dataset produced at an hourly timescale consisted of 19 variables (in five levels) per three CMIP6 models with five simulations (historical + four SSP projections) with 34 or 36 years per each one (Appendix A, Table A2). The high temporal and spatial resolution (up to one hour and 100 m) combined with the large number of variables made it necessary to divide the generated information into year-range files of approximately 100 MB, which includes all the variables of each vertical level to facilitate numerical computing. In total, this amounts to 111,606 files summing 977,668,560 hourly spatial fields with an average of 1068 points per domain. The three domains considered for daily scales amount to 52,866 files with 19,296,090 daily fields (Appendix A, Table A3). Therefore, 996,964,650 spatial fields were produced occupying approx. 16 TB plus intermediate 14 TB datasets.

As a reference of the past climate necessary for the statistical downscaling, the global reanalyses ERA5 (for atmospheric variables) and ERA5-Land (surface variables) were selected. They are the latest reanalysis datasets from the European Centre for Medium-Range Weather Forecasts (ECMWF), which offer enhanced spatial and temporal resolutions compared to previous versions. These were selected because they cover the geographical area pertinent to the DISTENDER project and since their simulations are recognized as among the most reliable available (Copernicus-C3S, 2024).

3. Downscaling techniques

3.1. Statistical approaches

3.1.1. General description of the three stages

To date, there is no climate data publicly available at km- scale, $<4\,$ km, over Europe under future scenarios either by dynamical or statistical downscale approaches. At the beginning of the project, downscaling of CMIP6 projections was not available yet for Europe (Euro-CORDEX 2022) and they typically provide data at regional scale, i.,e $10{-}12\,$ km, while DISTENDER require climate data on local scale. For statistical downscaling, previous products did not provide hourly resolution for the climate projections (e.g. the Chelsa project, Brun et al., 2022). Other

daily products were generated only after the definition of the DISTENDER products (e.g. Copernicus-C3S, 2022).

The statistical downscaling method used in DISTENDER combine well-known techniques, widely implemented in previous international projects such as STARDEX (2001–2004), RESCCUE (2016–2020), ECCLIPSE (2019–2022), CRISI-ADAPT2 (2019–2022) and FIREURISK (2021–2025) (Ribalaygua et al., 2013; Monjo et al., 2021, Monjo et al., 2023; Torres et al., 2020; Hetzer et al., 2024). The method consists of three stages (Fig. 1): (1) Parametric quantile mapping to obtain the same spatial resolution that the reanalysis at a daily scale, (b) Hourly time scaling based on analogy by spatial patterns and a transference of daily extremes to hourly curves from the most similar day in the reanalysis, and (c) Geostatistical downscaling hour-by-hour applied to the spatial fields. The reference time period used in SDS was the 1981–2014 period, bounded by the last year of the Historical experiments (1951–2014) and the starting of most observed data (about 1980).

3.1.2. First stage: parametric quantile mapping at the reanalysis resolution

3.1.2.1. Approach description. In DISTENDER, past and future climate simulations are generated using a downscaling technique based on transfer functions, specifically parametric quantile–quantile mapping (Benestad, 2010; Monjo et al., 2014, Monjo et al., 2023), with ERA5-Land as the reference dataset (approximately 8 km spatial resolution). This method is applied systematically to all climate variables, time series, and projections (10 climate models \times 4 SSPs, when available) using a two-step process:

- First, for a given historical experiment, each daily climate variable is downscaled to the corresponding ERA5-Land reference grid point. This is achieved by obtaining the Empirical Cumulative Distribution Function (ECDF) of the reanalysis data, in our common reference time period (1981–2014), and comparing with that of the historical experiment from each climate model, which has been previously bilinearly interpolated. This comparison allows for the derivation of a quantile–quantile mapping, which is then used to fit parametric functions. In our approach, five-parameter polynomial curves (y(x) = a₀ + a₁x + ... + a₄x⁴) are selected to optimize computational efficiency, as they require less processing time compared to the exponential distributions proposed by Monjo et al. (2014, 2016).
- In the final step, these parametric functions are applied to correct the SSP-RCP projections at a daily scale over the entire time series, without differentiation by month or season. The resulting downscaled projections are generated for a grid encompassing all European countries, maintaining the same spatial resolution as ERA5-Land.

The selection of transfer functions depends on the statistical characteristics of each climate variable. If a variable follows a smoother distribution (e.g., linear uniform or Gaussian, as seen in temperature and humidity), the transfer function is based on increments (f):

$$f: S(ERA5) \rightarrow S(ERA5) - S(HIST)$$

RES = MOD + f(MOD)

where S represents the value-sorting function. Conversely, if the variable follows an exponential-type distribution (e.g., log-normal, Weibull, or gamma; see Fig. 2), the function is fitted using multiplicative factors (g)

Table 2Information about the three CMIP6 climate models selected for DISTENDER.

CMIP6 Model	Climate Change level	AGM horiz. resolution	Responsible centre	Reference
CanESM5	Upper (75 %)	2,812° x 2,790°	Canadian Centre for Climate Modelling & Analysis	Swart et al. (2019)
EC-EARTH3-Veg	Medium (50 %)	0,703° x 0,702°	EC-EARTH Consortium	Döscher et al. (2022)
MPI-ESM1-2-HR	Lower (25 %)	0,938° x 0,935°	Max-Planck Institute for Meteorology (MPI-M)	Von Storch et al. (2017)

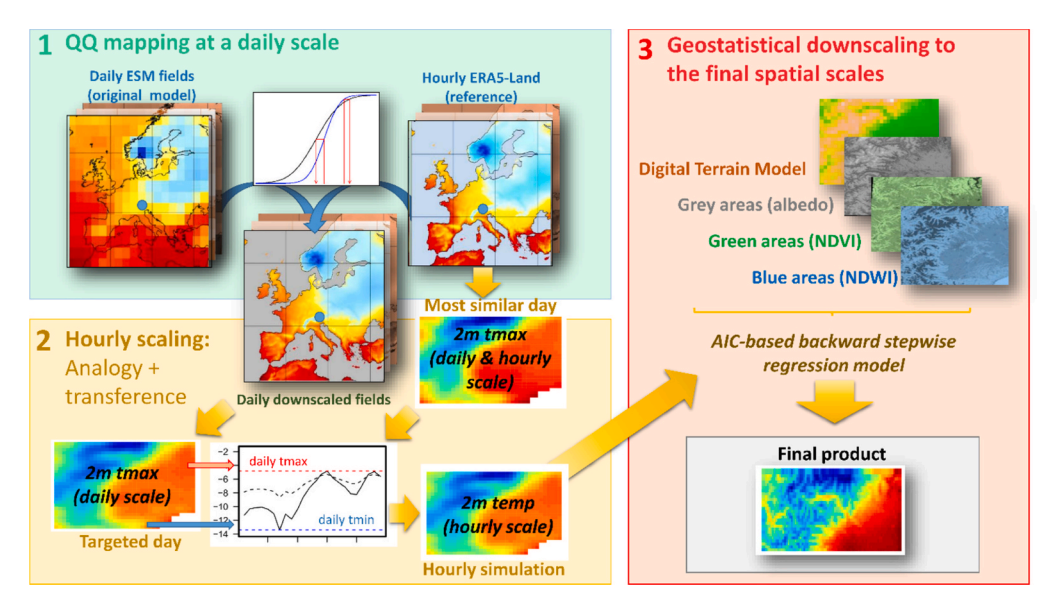


Fig. 1. Summary of the main three stages considered in downscaling of the climate model outputs for a particular core case study (e.g., Città Metropolitana di Torino, CMTo): (1) The first stage is common for all the DISTENDER domains and is based on a parametric quantile mapping applied at the same spatial resolution that the reference ERA5-Land reanalysis. (2) The second stage consists of an analogy and a transference of curves: The analogue stratification (e.g., Euclidean distance of relative spatial patterns) serves to find the most similar day for each targeted day by comparing maximum/minimum daily value of the reference reanalysis and the ESM fields. Then a transference function is applied to force the reference hourly curve to the maximum/minimum value of the targeted day. (3) The final stage is a classical geostatistical downscaling by Akaike Information Criterion (AIC)-based backward stepwise regression model. In our case, the used predictors were topographic variables calculated in a Digital Terrain Model (elevation, distance to the seas), albedo to represent 'grey areas', Normalized Difference Vegetation Index (NDVI) to represent 'green areas' and Normalized Difference + Water Index (NDWI) to represent 'blue areas', selected as three land-cover dimensions. (For interpretation of the references to colour in this figure legend, the reader is referred to the web version of this article.)

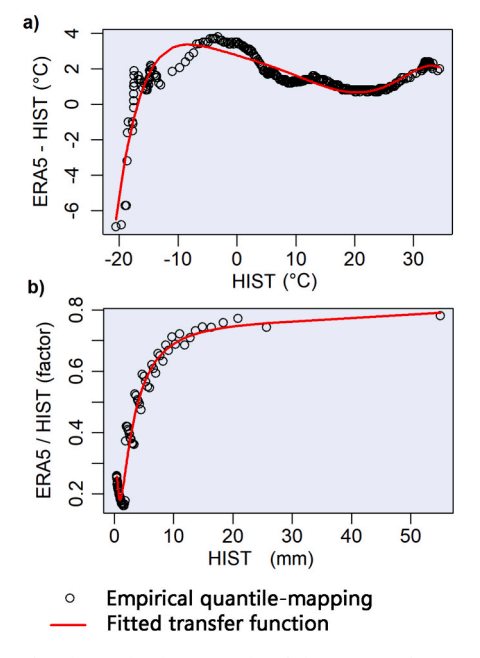


Fig. 2. Example of transfer functions fitted for empirical quantile-mapping values of: a) gaussian variables (temperature) and b) exponential-type variables (precipitation). This example corresponds to the historical exponential data (HIST) from a grid point of Austria (47.27°N, 11.39°E) for EC-EARTH3-Veg compared to the closest grid point of the ERA5 reanalysis.

derived from the comparison of target quantile values (from *HIST*) with their corresponding reference quantiles (from logarithmic values of *ERA5*):

 $g: S(log(ERA5)) \rightarrow S(ERA5)/S(HIST)$, for ERA5 > 0 and HIST > 0

$$RES = MOD*g(MOD)$$

where *RES* is the resulting (daily) climate scenarios with the desired spatial resolution, and *MOD* is the merge of historical (*HIST*) and projections (*PROJ*). This implies that extreme values—when *MOD* falls outside the distribution tails of *HIST*—are adjusted using the same increment (*f*) or factor (g) as those derived from the empirical tails of the training sample (*HIST*). This approach can be directly applied to classical scalar variables such as temperature, precipitation, humidity, and pressure, whether they follow smooth or exponential distributions. The method utilizes polynomial fits of up to the 6th degree, applied to either linear or logarithmic factors. Since climate change leads to values extending beyond historical distribution tails, these out-of-range values are corrected using the final truncated factor from the tail mapping (*f* or g).

However, some variables required additional procedures (Table 2). This approach applies to vectorial variables (wind) and flux variables (e. g., short- and long-wave downward radiation). Finally, additionally to the annual and seasonal bias, a Kolmogorov-Smirnov test (Sekhon, 2010) was applied to analyse the model performance.

3.1.2.2. Approach motivation, advantages and limitations. The parametric quantile mapping approach was chosen for its balance between statistical robustness, flexibility across variables, and computational efficiency over large datasets, as it produced good results in the Cost VALUE comparative (Gutiérrez et al., 2018). By explicitly fitting transfer functions to match the cumulative distribution functions of model outputs to reanalysis data, it ensures correction of systematic biases not only in means but in higher quantiles, which is especially important for extreme events (Monjo et al., 2014, 2016, Monjo et al., 2023).

The parametric form (polynomial curves) reduces storage and computational demands compared to non-parametric empirical quantile mapping, which is essential for handling multi-model, multi-scenario daily projections over Europe. Moreover, by distinguishing between additive and multiplicative correction schemes depending on variable

distribution (smooth vs. exponential), the method accommodates a wide range of physical variables while preserving their statistical characteristics. However, the approach also has limitations. It assumes stationary bias structures between historical and future periods, which may not fully hold under strong climate change. It also relies on the quality and representativeness of the reanalysis reference data (ERA5-Land), which can carry its own uncertainties. Finally, the approach can be less effective in correcting spatial or temporal dependencies, as it operates point-wise on the grid, although wind components are treated jointly to address directional dependencies.

3.1.3. Second stage: analogue-based approach for hourly timescale

3.1.3.1. Selected method: Gridded dataset as a reference. CMIP6 model outputs do not have hourly data but they have 6-hourly and daily fields, so it is not possible to directly apply a quantile mapping at hourly scale here. Therefore, to obtain gridded products for all the DISTENDER domains, a second stage used the daily outouts of the first stage (Sec, 3.1.2) and the hourly fields from ERA5 and ERA5-Land reanalyses as references, following three steps:

Analogue stratification: A stratification was performed by using a Euclidean distance of relative spatial patterns (root of standardized square differences). This geometrical technique allows to order all the reference days (in the past) of the reanalyses according to their similarity with each 'targeted day'. Specifically, we found the most similar day for each targeted day (from ESM fields) by comparing relative spatial patterns of daily-aggregated values. For instance, maximum and minimum temperatures were selected to describe the atmospheric configuration (clear-sky or cloudy-day patterns) to capture typical hourly curves for each configuration and region. To ensure physical consistency among the different variables, the same analogous day was selected for all the variables simulated.

Parametric daily-to-hourly scaling: For each downscaled climate projection (to the ERA5-Land grid) and for all climate variables, every targeted daily field was scaled to an hourly resolution by using the reference features of the ERA5-Land. Hence, the hourly curve of the climate variables (e.g., temperature, humidity, and wind) was obtained from the most similar day (of ERA-Land reanalysis) to the target day. A parametric transfer function is then applied between the targeted daily field (e.g. maximum and minimum daily values) to the hourly fields of the most similar day in the past.

Filtering of jumps: Since every day is simulated separately, possible jumps may occur, which are smoothed by jointly filtering the three last hours of each day and the first three hours of the following day. The used filter is a spline-weighting function between the average trend in these six hours and their original values, applying the higher smoothing to the last-first hours (23 h and 00 h).

3.1.3.2. Alternative method: point observations as a reference. Similarly to the dynamical approaches, statistical grid-based methods have coherent and robust spatial distributions, but they can underestimate extreme values (distribution tails) of some climate variables, especially for precipitation and wind. To complement this issue, an alternative to the DISTENDER approach is generating climate scenarios at a local scale by using statistics of direct observations, measured in a point (e.g. weather station, rain gauge, hygrometer and thermometer, among others) and then applying point-observation-based bias adjustment or perfect prognosis approaches.

If there is a sufficient station network density, statistical downscaling of ESM translates general atmospheric configurations from *large-scale predictor fields* (of ESM simulations) to local climate information obtained from *surface point observations*. The recommended method is a two-step analogue-transference approach which combines an analogue stratification and parametric transference functions. This method has been validated in international comparisons for climate models and

reanalysis (Ribalaygua et al., 2013; Gutiérrez et al., 2018). The outputs of this spatial downscaling are time series representing the climate of the reference points, the same points as the observatories or the reanalysis grid points used for training the method.

3.1.4. Third stage: geostatistical downscaling to the final spatial scales

At this stage, a *topography-based multi-linear interpolation* was applied to the 8 km-resolution downscaled model outputs (trained with the time series from the ERA5-Land reanalysis) to generate a finer resolution. Particularly, for each climate variable simulated by the CMIP6 models, the last stage is applied according to three steps:

1) For all variables (Table 2) and each projected day (with 0.073°×0.073° resolution, ~8 km), a geostatistical interpolation allowed to obtain a high-resolution grid by using AIC-based stepwise multi-linear regression (Venables and Ripley, 2002) with geographical variables (altitude, latitude, longitude, distance to the Atlantic Ocean and Mediterranean Sea) and Corine-2018 (EEA, 2020) land-cover variables (albedo, NDVI, NDWI; Table 3) used as predictors.

Table 3Daily variables generated by statistical downscaling and the specific procedures.

Type	Variable	Specific procedures
2 m air temperature (°C)	TMax: Maximum temperature TMin: Minimum temperature	These variables are directly obtained using parametric quantile mapping, assuming a smooth distribution. Additionally, mean temperature is defined as: TMean = (TMax + TMin)/2
2 m air humidity (%)	HRMax: Maximum relative humidity HRMin: Minimum relative humidity	It is directly corrected by parametric quantile mapping (smooth distribution). A post-process was done to limit values within the physically meaningful range of 0 % to 100 %.
surface precipitation (mm)	tpr: Total daily (24-h) precipitation	This variable is directly generated using parametric quantile mapping, assuming an exponential probability function. No additional adjustments are required because the mathematical process does not produce negative values.
10 m Wind (m/s)	W: Mean wind module. U, V: Wind components	The wind module (W), defined as $W = \sqrt{U^2 + V^2}$, is directly obtained as an exponential variable. However, since the U and V components are not entirely independent —due to certain wind directions being more frequent as a result of topographical influences—, it is essential to account for this dependency by considering: - Mutual dependent contribution $\langle U \rangle = F(\langle V \rangle)$, that is the "predictable contribution" of U as a function of V and vice versa, where F is a linear function fitted. - Residual contributions, which are $[U]:=U-\langle U \rangle$ and $[V]:=V-\langle V \rangle$. Therefore, three variables are corrected as smooth distributions: $[U]$, $[V]$, and $\langle X \rangle$ (representing either $\langle U \rangle$ or $\langle V \rangle$). The corrected wind components are then obtained as $V'=[V]'+\langle V \rangle$ and $U'=[U]+F(\langle V' \rangle)$. Finally, the corrected components U' and U' are normalized to derive the wind direction θ , and the final wind components are computed as $U''=W'$
Solar radiation (W·m ⁻²)	LWD: Long-wave down radiation SWD: Short-wave down radiation	cos θ and V'' = W' sin θ The transfer function is applied to the total solar radiation from ERA5-Land. Subsequently, long-wave and short-wave radiation components are separated based on the original ratio provided by the climate model.

- 2) Similarly, for each day, residual errors of the AIC-based stepwise regression are interpolated from the original grid $(0.073^{\circ} \times 0.073^{\circ})$ to the final grid (e.g., $1000 \text{ m} \times 1000 \text{ m}$ or $30 \text{ m} \times 30 \text{ m})$ by using a simple bilinear model (using latitude and longitude as predictors).
- 3) Finally, the projected value for each day is obtained by adding the result of 1) and 2), obtaining climate scenarios in the high-resolution grid at an hourly timescale (Fig. 3).

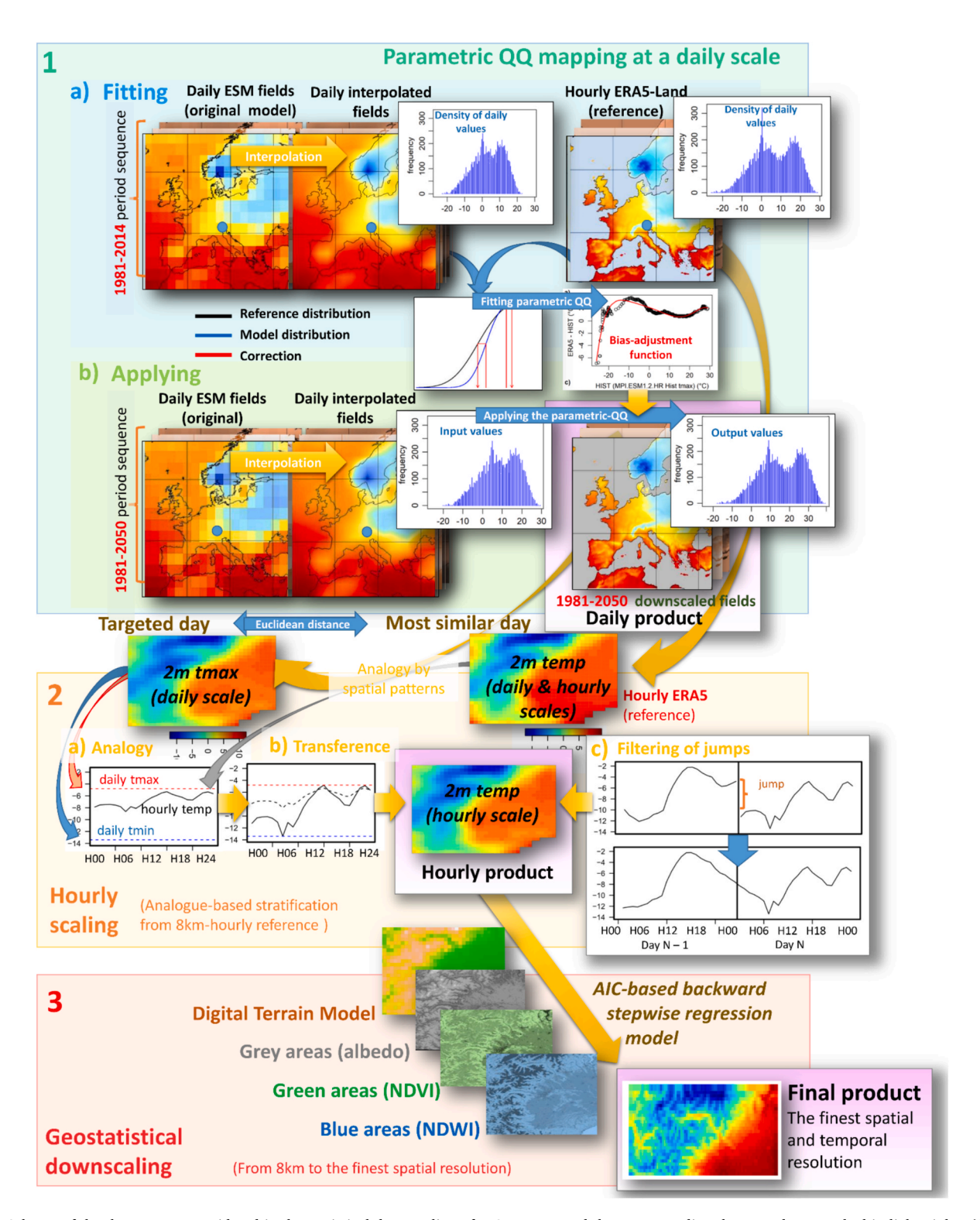


Fig. 3. Scheme of the three stages considered in the statistical downscaling of DISTENDER and the corresponding three products marked in light violet: (1) Daily products for Europe at the same spatial resolution as the ERA5-Land reanalysis: (2) Hourly products obtained by transferring of the hourly curve found in the most similar day (reanalysis) to each targeted day (ESM fields); (3) Final product with the finest spatial and temporal resolutions (achieved by geostatistical downscaling hour by hour). (For interpretation of the references to colour in this figure legend, the reader is referred to the web version of this article.)

3.2. Dynamical downscaling

3.2.1. General description

Dynamical downscaling is an approach to obtain high-resolution climate simulations using regional climate models (RCMs) or limited area models running with ESM outputs as lateral boundary forcing (Trzaska and Schnarr, 2014). Since it is based on the physical laws of fluid mechanics and thermodynamics, dynamical downscaling has supremacy to hold true even in changing climate conditions. However, the limitation is that it is computationally more expensive than statistical downscaling (Tang et al., 2016).

State-of-art dynamical downscaling efforts encompass European initiatives such as Med-CORDEX, EURO-CORDEX, and the European Climate Prediction (EUCP) system project. Dynamical downscaling of CMIP5 is available from these projects; however, the projections of the most recent generation of intercomparison project, i.e. CMIP6, were under completion in dynamical downscaling at the beginning of this project (Dyrrdal et al., 2018). In addition, when it becomes available, it will provide information at regional scale, while DISTENDER aims for climate information at local scale, i.e., higher resolution.

Therefore, in DISTENDER, dynamical downscaling (DDS) of the CMIP6 EC-Earth3-Veg over Med-CORDEX domain (WCRP MedCORDEX, http://www.medcordex.eu) at km-scale (also known as convection-permitting, i.e. grid-spacing < 4 km) was performed. The decided spatial resolution for DDS is 3.9 km which is expected to sufficiently resolve important processes to produce climate information at local scale for the DISTENDER core case studies and was just computationally afforable. The climate model and simulation design are described in the following sub-sections.

3.2.2. Model features

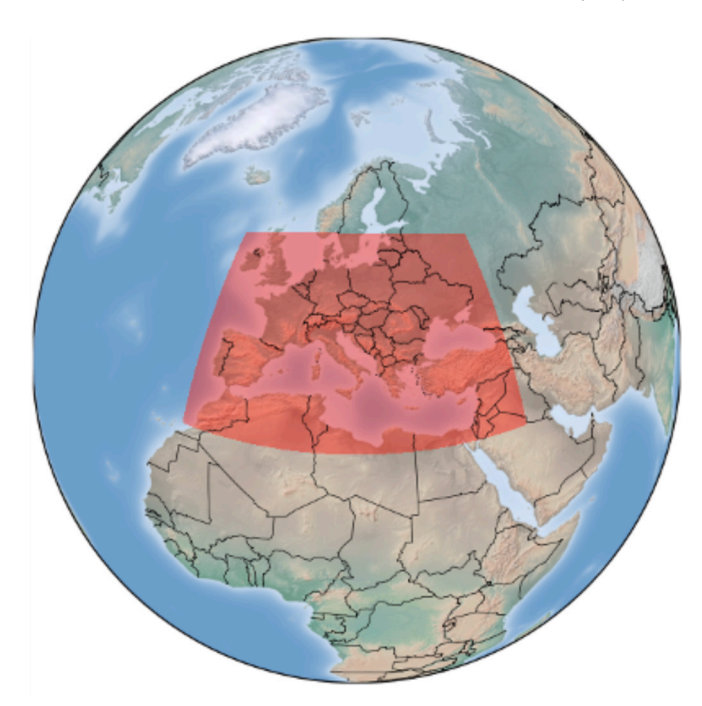
The ICOsahedral Nonhydrostatic (ICON) (Zängl et al. (2015, 2022) model is selected for dynamical downscaling within the DISTENDER project. ICON is an outcome of a collaboration between Deutscher Wetterdienst (DWD) and Max Planck Institute for Meteorology (MPI-M). It can be used for both numerical weather prediction and climate simulations. As the name suggests, ICON's numerical grid is based on the icosahedron, i.e., the spatial area is divided into a triangular mesh and has the terrain-following vertical coordinate. The model dynamics involves fluid motion equations integrated forward in time. Additional key components of ICON are numerical advection of atmospheric quantities like cloud water and humidity, and parameterizations of unresolved physical processes. The temporal integration in ICON utilizes a combination of the Matsuno scheme and the Heun scheme (Prill et al., 2022).

ICON for climate simulations can be applied in either a global set-up or a limited-area set-up driven by both global reanalyses and global climate projections. Here, we use the limited-area model configuration of ICON-CLM version 2.6.5, which is actively developed in the CLM-Community (http://www.clm-community.eu) and is a successor of COSMO-CLM (successfully applied before and still used in many EU projects like ENSEMBLES, BRAHMATWINN, SOCLIMPACT, EUCP). The regional domain selected for dynamical downscaling is alike CORDEX region 12 (i.e., Mediterranean basin, Med-CORDEX, https://www.medcordex.eu), as shown in Fig. 4. It allows producing the required meteorological variables, especially for the core-case studies sub-domains. In addition to the suitable configuration of ICON-CLM to our domain, we used TERRA-URB land-surface scheme (Wouters et al., 2017) due to its more detailed representation of urban and urban change effects.

Due to computational constraints (i.e., computing and storage resources), dynamical downscaling simulations in DISTENDER driven by only one CMIP6 model, EC-Earth3-Veg, that has medium sensitivity to climate change compared MPI-ESM1-2-HR and CanESM5 models.

Further, the temporal coverage of dynamical downscaling simulation is 11 years each; the first year is considered as a spin-up period.

Analogous to the statistical downscaling, a historical simulation and four SSPs future simulations have been performed (Table 4). Table 5.



 $\begin{tabular}{ll} {\bf Fig.} & {\bf 4.} {\rm \ The \ \ model \ \ domain \ \ selected \ \ for \ \ dynamical \ \ downscaling \ \ using \ \ ICON-CLM. \end{tabular}$

A 10-year present simulation by dynamical downscaling (DDS) of EC-EARTH3-Veg (spin-up 2010, historical 2011–2014, SSP126 2015–2020) was primarily analysed for precipitation and temperature bias in the seasonal and annual mean. For a better bias assessment and adjustment of the DDS outputs, gridded observational data for the European region (E-OBS, Cornes et al 2018) is used along with the provided boundary forcing (EC-EARTH3-Veg).

3.2.3. Post-processing

The output of the DDS simulations have been post-processed to fit the defined domains of DISTENDER core case studies as well as the spatial and temporal resolutions (Table A1). Post-processing steps also included bias adjustment for the near-surface temperature and precipitation to the ICON-CLM output (Fig. 5). It is well known that regional model simulations suffer from two types of biases 1) inherited from driving ESM and 2) due to model physics. These biases have the potential to further influence the performance of impact models running on input from regional climate models (Seaby et al., 2013). However, different bias-adjustment techniques can be employed to meteorological variables, especially precipitation and temperature, to improve the quality of climate data produced by RCMs.

We used the gridded observational E-OBS (Cornes et al 2018) data as a reference for precipitation bias adjustment. Further, due to data scarcity in the southern Mediterranean by E-OBS, the IMREG satellite (https://disc.gsfc.nasa.gov/datasets/GPM_3IMERGDF_07/summary)

has been used to fill in missing reference data. E-OBS is an ensemble dataset available on a 0.1 degree regular grid for daily precipitation sum, among other climate variables. Version 27.0 has been used here. For temperature, we used instead the CRU TS dataset (Harris et al., 2020), version 4.07 https://crudata.uea.ac.uk/cru/data/hrg/) as a reference for bias adjustment, The reason is in known E-OBS infrequent issues in representing correct daily maximum and minimum temperatures (https://surfobs.climate.copernicus.eu/userguidance/known_iss_ues_eobs.php). The CRU TS dataset is a gridded observational-based dataset over land at 0.5°x0.5° grid-space, and monthly time resolution. To be able to apply bias-adjustment over sea, we used 2-meter temperature over sea from ERA5 data (Hersbach et al., 2020).

The casuistic between SDS and DDS is distinct mainly due to the use

Table 4
Assignment between ten simplified land cover types and three physical predictors for a geostatistical downscaling (albedo, NDVI and NDWI). As input, we used 44 Corine-2018 categories (EEA 2020).

Simplified land cover type	Gathering of land covers	Albedo	NDVI	NDWI
urban	1,2,3,4,5,6,7,8,9	0.2	0.08	0.3
green urban	10,11	0.15	0.75	0.6
arable lands	12,13,14,15,16,17,18,19,20,21	0.3	0.3	0.45
forest agroforest	22,23,24,25	0.13	0.8	0.7
grasslands moors shrub	26,27,28,29	0.3	0.3	0.55
sands bare rocks	30,31,32	0.4	0.4	0.15
burnt areas	33	0.05	0.05	0.2
glaciers snow	34	0.7	0.7	0.15
marshes peat bogs	35,36,37	0.15	0.2	0.6
water courses & lagoons	38,39,40,41,42,43,44	0.1	0.05	0.9
Corine-2018 categories: 1	continuous_urban_fabric	23	broad_leave	d_forest
2	discontinuous_urban_fabric	24	coniferous_f	orest
3	industrial_or_commercial_units	25	mixed_fores	t
4	road_&railnetworks_&associated_land	26	natural_gras	slands
5	port_areas	27	moors_and_l	neathland
6	airports	28	sclerophyllo	ous_vegetation
7	mineral_extraction_sites	29	transitional	woodland_shrub
8	dump_sites	30	beaches_dur	nes_sands
9	construction_sites	31	bare_rocks	
10	green_urban_areas	32	sparsely_veg	getated_areas
11	sport_and_leisure_facilities	33	burnt_areas	
12	non_irrigated_arable_land	34	glaciers_and	_perpetual_snow
13	permanently_irrigated_land	35	inland_mars	hes
14	rice_fields	36	peat_bogs	
15	vineyards	37	salt_marshes	S
16	fruit_trees_and_berry_plantations	38	salines	
17	olive_groves	39	intertidal_fla	ats
18	pastures	40	water_cours	es
19	annual_crops_and_permanent_crops	41	water_bodie	S
20	complex_cultivation_patterns	42	coastal_lago	ons
21	land_principally_occupied_by_agriculture_with_significant_natural_areas	43	estuaries	
22	agro_forestry_areas	44	sea_and_oce	an.

Table 5Simulation plan for Dynamical-downscaling set-up within DISTENDER.

Simulation No.	Period	Forcing/LBCs
1		
	Historical simulation	EC-EARTH3-Veg
	(1-year spin up, 2011–2020)	
2.	Future Projections	EC-EARTH3-Veg/SSP126
	(1-year spin up, 2041-2050)	EC-EARTH3-Veg/SSP245
		EC-EARTH3-Veg/SSP370
		EC-EARTH3-Veg/SSP585

of ERA5 and ERA5-Land reanalyses as references for SDS, which mostly bias-corrects all the variables at different vertical levels, while DDS directly produces physically-consistent fields at all the levels avoiding the need of using the reanalysis dataset to obtain all its variables. Therefore, by direct result (effect of the training process from the reanalysis data), SDS outputs are practically unbiased, so no additional procedures are required in contrast to the significant systematic errors in temperature and precipitation that are usually obtained from DDS. Instead of reanalysis, regular grids of observations (such as E-OBS and CRU TS) are more commonly used to correct bias of DDS outputs, except for the maritime areas

For the DDS in DISTENDER, we assessed different methods and opted for relatively simple, but robust bias-adjustment methods for precipitation and temperature, respectively;

a) Precipitation bias-adjustment. A simple method known as local intensity scaling (Schmidli et al., 2006, Dobler and Ahrens, 2008) was used to adjust model produced precipitation as per observation in the historical period. The simulated precipitation was adjusted at daily scale and the coarser spatial resolution of the observational reference dataset (i.e., 0.1°). The coarsened simulated data is adjusted in two main steps: The first step is to adjust the frequency of

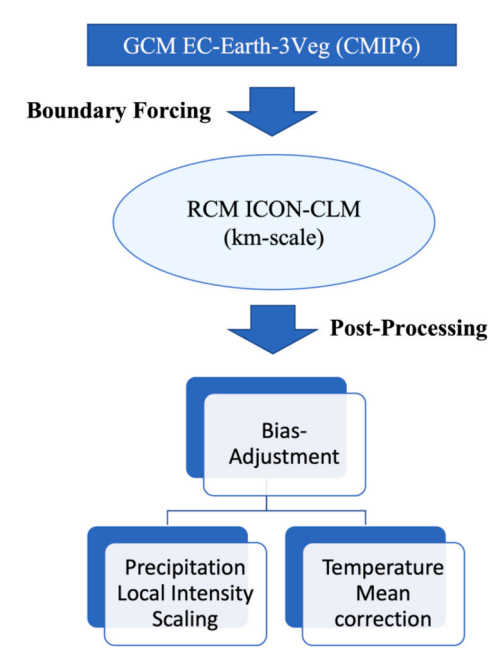


Fig. 5. Schematic of Dynamical-Downscaling approach within DISTENDER.

wet days (i.e., days with observed precipitation ≥ 0.1 mm/day). This is achieved by adjusting the threshold of the simulated wet days (the model typically simulates too many wet days in Europe which leads to spatially varying thresholds larger than 0.1 mm/day). The second step is a multiplicative scaling of the precipitation intensities with the ratio of the means of simulated and observed wet day intensities. The scaling factors vary in space around the value 1. After coarse-

grid adjustment the fine-grid multiplicative increments are applied to the simulated precipitation again. The same adjustment using the same wet day thresholds and scaling factors is applied to the future period simulation.

b) **Temperature bias-adjustment.** The applied bias-adjustment for temperature is based on correcting daily minimum temperature and diurnal temperature range (DTR). Considering DTR in temperature's BA helps maintain physically realistic relationships between

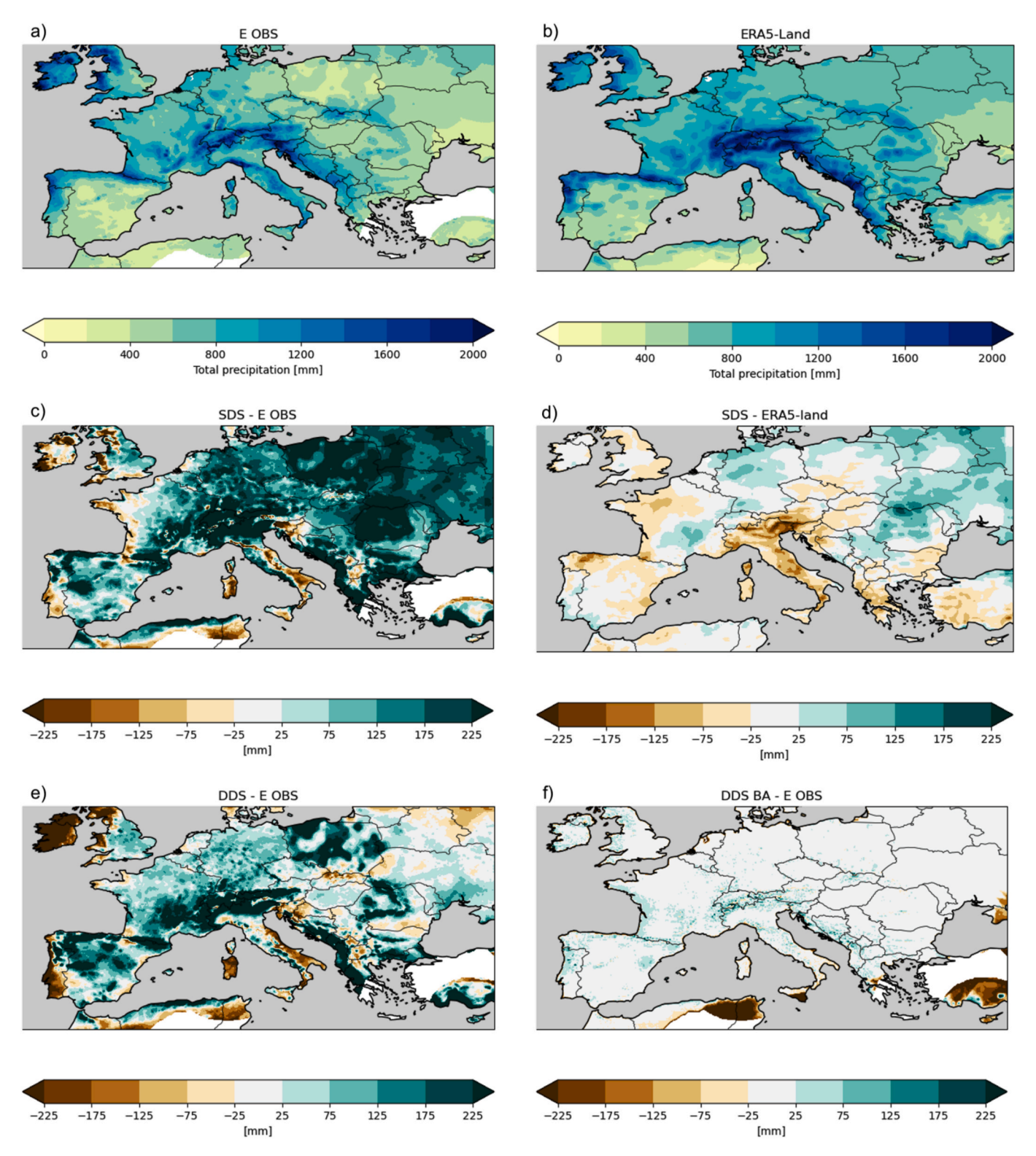


Fig. 6. Mean values of precipitation (mm) in the 2011–2020 period for the annual period according to E-OBS (top left) and ERA5-Land (top right) and bias (mm) of the EC-EARTH3-Veg downscaled with the statistical approach (SDS, middle panels) and dynamical approach (DDS, bottom panels). On the right, the statistical downscaling is compared to ERA5-Land since it was the basis for the daily quantile mapping, while the bias adjustment of the dynamical downscaling (DDS BA) was performed with E-OBS in Europe. The historical experiment of EC-EARTH3-Veg was extended with the SSP1-2.6 projection to complete the 2011–2020 period in both SDS and DDS approaches.

maximum and minimum temperatures, and is widely used for adjusting temperature biases from climate models' output (Cucchi et al., 2022; Lange, 2021). The minimum and maximum temperatures in the historical simulation are coarsened to the grid of the observational reference $(0.5^{\circ}$, monthly). This allows the determination of an additive minimum temperature bias and a multiplicative bias of diurnal temperature range. These coarse-grid biases are applied in the adjustment of the model-grid data. The same adjustment using the same biases are applied to the future period simulation.

Finally, the model data with 3.9 km grid-spacing for all variables (including bias-adjusted precipitation and temperature) was interpolated to the required spatial resolutions of 9 km and 3 km (Table A1) for core-case studies.

4. Results and discussion

4.1. Historical simulation assessment

When SDS is considered for the three climate models, the performance analysis concluded that the downscaled historical experiment of EC-EARTH3-Veg presented the smallest bias for precipitation compared to ERA5-Land in the 1981–2014 period (not shown). The annual precipitation distribution passed the KS test at a daily scale for the three downscaled climate models. At a seasonal scale, summer is the worst simulated period, with July and August systematically failing out the KS tests for the downscaled EC-EARTH3-Veg, especially for Guimaraes. Finally, spring and winter seasons are adequately simulated by the downscaled EC-EARTH3-Veg according to the KS test compared to ERA5-Land (p-value > 0.05).

To compare the SDS and DDS skills in the past simulation, the historical experiment of the climate models was extended with the SSP1-2.6 projection, obtaining a complete common period of 10 years (2011-2020). Systematically, the E-OBS reference estimates a lower precipitation amount for the mountainous regions than the ERA5-Land reanalysis for the 2011-2020 period (Fig. 6 top). With this difference, most patterns found in the bias field of DDS and SDS (Fig. 6 left center and bottom) can be explained by two reasons. On the one hand, the deviation between EOBS and ERA5-land is consistent with SDS bias toward EOBS due to the SDS dependence on ERA5-land, and on the other hand, the parameters of EC-EARTH3-Veg (IFS cycle 36r4) are partially shared with those ones used in the ECMWF simulations of the ERA5 and ERA5-Land (IFS cvcle 45r1, https://confluence.ecmwf. int/display/CKB/ERA5-Land). Therefore, SDS generally displays higher relative biases in precipitation with respect to E-OBS (up to \pm 50 % in Eastern Europe) than when it is compared to ERA5-Land (smaller than \pm 20 %, Fig. 6). This overestimation contrasts with DDS, which maintains reduced biases about \pm 10 % across large areas of Northern and Eastern Europe, reflecting a more constrained adjustment. Consistently with the above mentioned, a common underestimation is found for some areas (e.g. for Southern Portugal and Eastern Italy) when both methods are compared to E-OBS. However, for their corresponding biasadjustment (BA) basis (E-OBS in DDS-BA and ERA5-Land for SDS), they show more consistent results, which fluctuates typically around $-10\ \%$ to + 10 % depending on the region (Fig. 6 right center and bottom).

Concerning mean temperature, SDS of EC-EARTH3-Veg outputs showed negative bias downs to -2° C in Northeast Europe. The statistical downscaling product of the CanESM5 model is an intermediate case, with low bias during winter (slightly positive up to 1 °C in Central Europe) and negative bias during summer, especially in Spain (-1° C).

The simulated near-surface (2-meters) temperature from DDS was also compared to observations (CRU). As in precipitation, temperature output also suffers from biases inherited from boundary forcing. The raw EC-EARTH3-Veg and its corresponding DDS present a warm bias tendency in central and east-central parts of Europe. This bias is more

noticeable during summer in EC-EARTH3-Veg SDS simulation, whereas the bias magnitude is less for its DDS result. Also, some southern and central orographic regions simulated by SDS have a cold bias during winter. In any case, the seasonal bias is not statistically significant for the 10-year historical simulation of the DDS, which was short due to computational limitations.

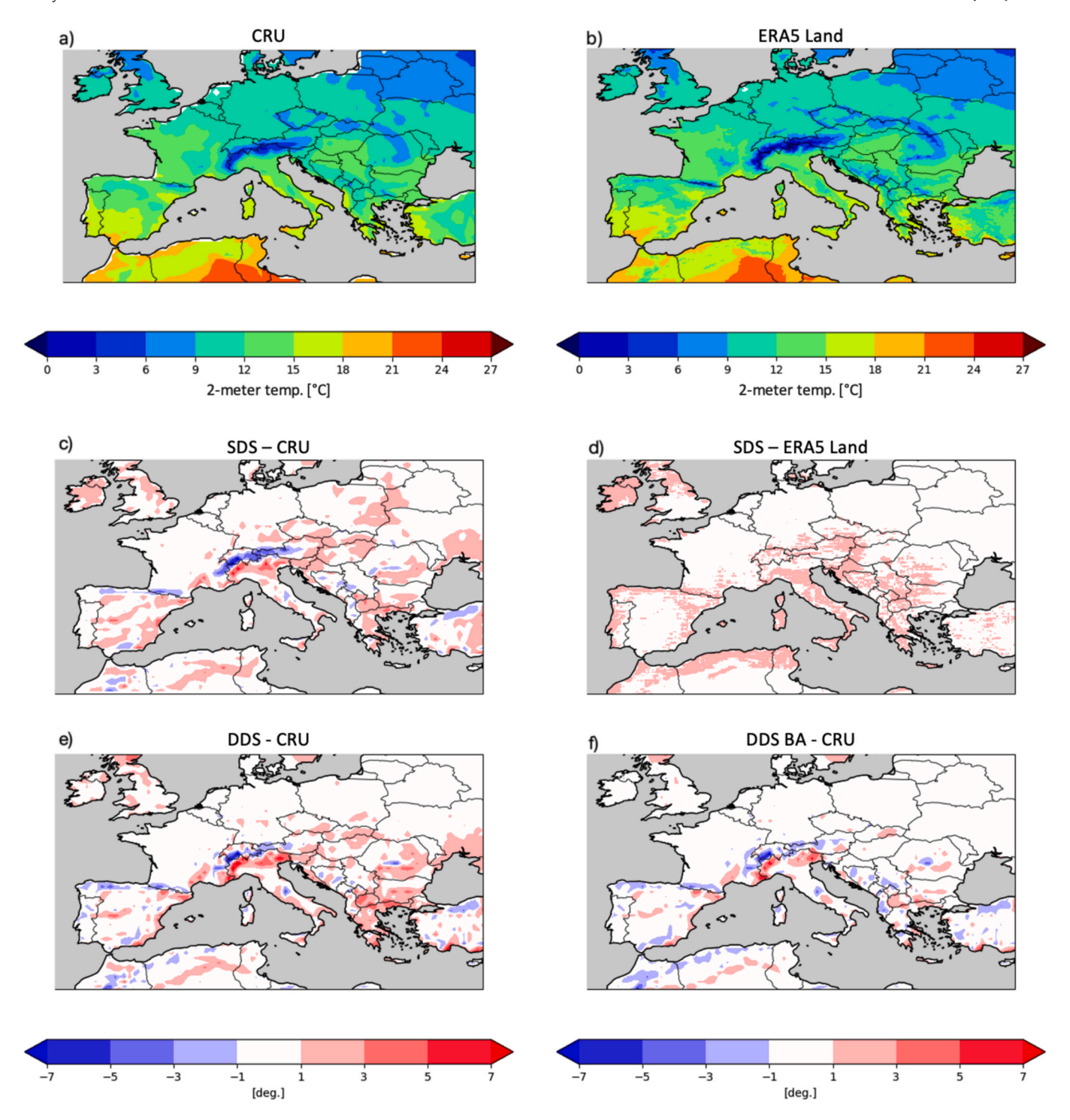
When comparing both downscaling methods with the respective reference bases (ERA5-Land for SDS and CRU for DDS BA), the systematic error of SDS is lower than DDS at the elevated regions such as the Alps (about 3 or 5 $^{\circ}$ C of bias), which impacts close to the study case of the CMTo region. However, it is slightly higher (1 or 2 $^{\circ}$ C) in Southeastern Europe and northern British Isles (Fig. 7). A few nuances are also found at other regions of interest for DISTENDER, as this is the case in the Spanish Central Mountains of the Euraf region.

In summary, there are three main uncertainty sources in the bias when comparing SDS and DDS: First of all, they use a different training time period, since the limited computational resources of DDS forced it to produce a shorter period (2011-2020) than the used for SDS (1981–2014). Moreover, SDS is naturally compared to the ERA5-Land reanalysis as it has been used to train the SDS procedure in the 1981–2014 period. For this reason, SDS – ERA5-Land bias is expected to be larger in 2011-2020 than in the natural baseline of 1981-2014, but it significatively presents less bias than SDS - EOBS. Finally, SDS is not exactly unbiased with respect to ERA5-Land even in the 1981-2014 period because the procedure is based on a parametric quantile mapping (no empirical quantile transference). In order to correct climate projections, empirical quantile mapping (i.e. actually unbiased) cannot be applied because unobserved values in the future projections are truncated to actual observed values (from the past), which invalidates the method for climate change analysis. In contrast, the parametric approach avoids overfitting by capturing simpler transfer functions between the simulated and the observed CDFs. In particular, the use of four-parameter polynomials does not guarantee that the quantile mapping be unbiased but it avoids overfitting.

4.2. Climate projections

In the climate projections (2041–2050) driven by EC-EARTH3-Veg, both DDS BA and SDS agree on certain large-scale patterns, such as an increase in precipitation in Northern Europe and a decrease in Southern Europe. However, the magnitude of these changes differs. Under all the SSP scenarios, for example, both SDS and DDS project precipitation increases in Central Europe exceeding + 15 % or + 25 % relative to the historical period (2011-2020). Moreover, both methods consistently indicate wetter conditions in the Alpine regions but differ in the spatial extent of these increases, with DDS BA showing more localized intensification for the worst SSP scenarios (Fig. 8). Meanwhile, in Southern Europe, particularly over Spain and Italy, DDS projects decreases up to -30 %, whereas SDS suggests a more moderate reduction, around -15% to -20 %. Despite these differences, a consensual pattern emerges: a wetter north and a drier south across Europe, though the intensity and spatial variability of changes are notably method-dependent. This discrepancy could reflect DDS's sensitivity to dynamic atmospheric processes that would amplify responses (e.g. zonal circulation versus cyclogenesis frequency) under high-emission scenarios.

Concerning the temperature projections (Fig. 9), both methods show similar paths but some differences can be pointed out, specifically in SSP1-2.6. In this scenario the DDS BA method projects a uniform slight warming across Europe (+1°C), whereas the SDS method suggests cooler anomalies, particularly in Eastern Europe and the Balkans (down to -2.25 °C). For SSP2-4.5, both methods predict a general warming (+1.75 °C), but the SDS approach depicts more intense (+1.75 °C) warming in the southwest (North Africa region). On the other hand, the SSP3-7.0 scenario shows a slightly lower warming than which can be seen in the SSP2-4.5, with a similar warming rate in southern Europe, but even with a slight cooling around central Europe, in both DDS BA



 $\textbf{Fig. 7.} \ \, \textbf{The same as Fig. 9} \ \, \textbf{but for average temperature, while the reference dataset is CRU.}$

and SDS. This can be explained because of differences existing within each SSP which affect the initialization of the climate models. In this case, since the projections end before 2040 these differences can allow us to find this paradox in the near-term projections. Moreover, this could also be driven by the member used in GCM, so it would be necessary to use the ensemble member to reduce the uncertainty of the single member dependence. Finally, in the worst-case scenario (SSP5-8.5), both methods show substantial warming across Europe (>2.25 $^{\circ}$ C) with the DDS presenting a slightly smoother gradients, while SDS emphasizes greater warming, specially in the south and eastern areas (Spain, Italy and Balkan regions). Nevertheless, in the two methods a smoother

warming in the Atlantic façade can be expected for this high-emissions scenario (France and British Islands with a warming up to + 1.25 $^{\circ}\text{C})$ thanks to the temperate effect of the Atlantic Ocean.

As an example of detailed local scenarios for the DISTENDER core case studies, future projections of seasonal temperature are shown in Fig. 10. Topographic effects on temperature are more perceptible during the summer since maximum temperature is sensitive to the elevation differences, and the nuances at a high spatial resolution are captured by the SDS method. In consistency with previous studies, the summer is also the season with more increase in temperature by 2050, up to $+\,5^{\circ}\mathrm{C}$ under the SSP5-8.5 scenario. However, a higher multidecadal variability

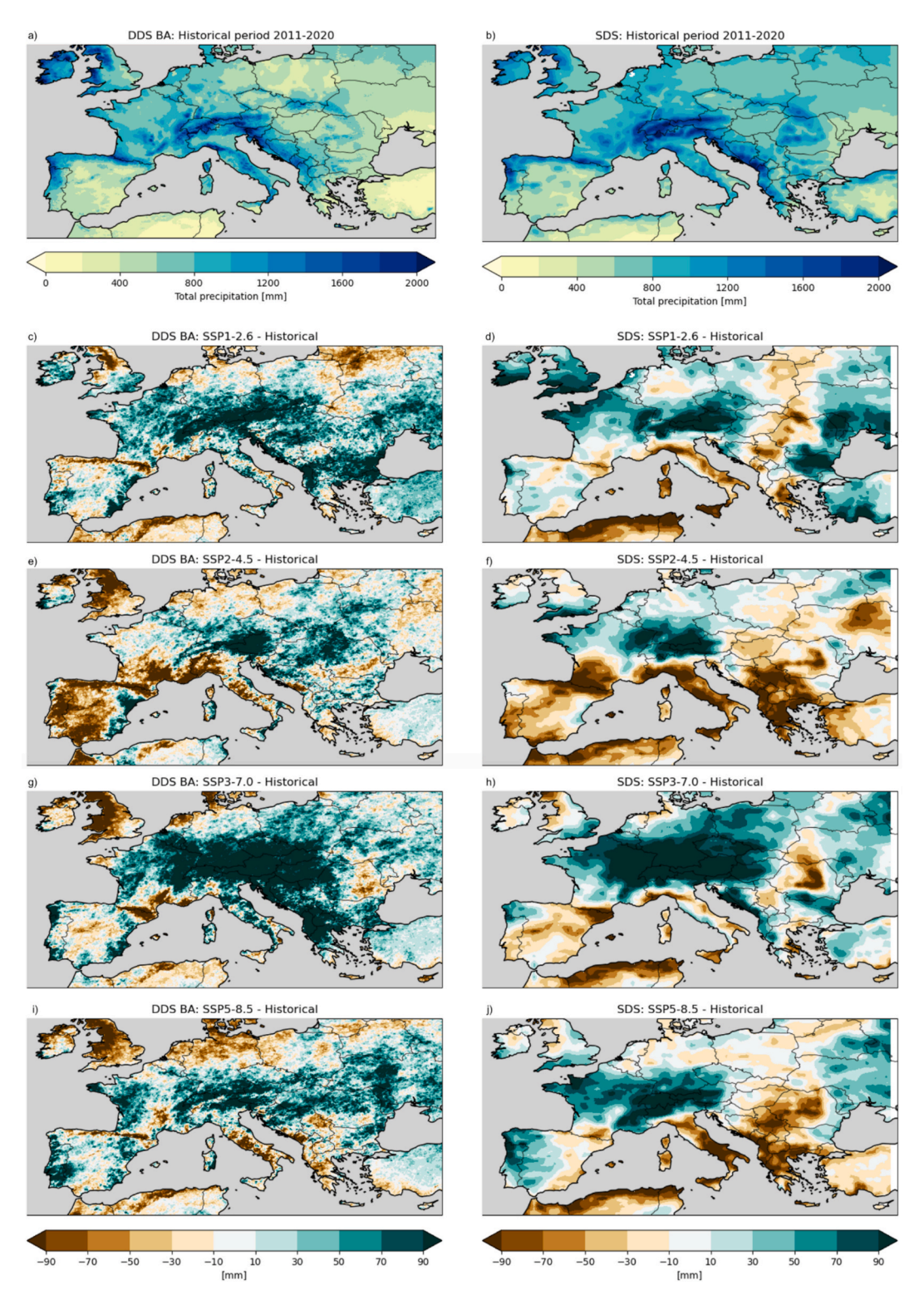


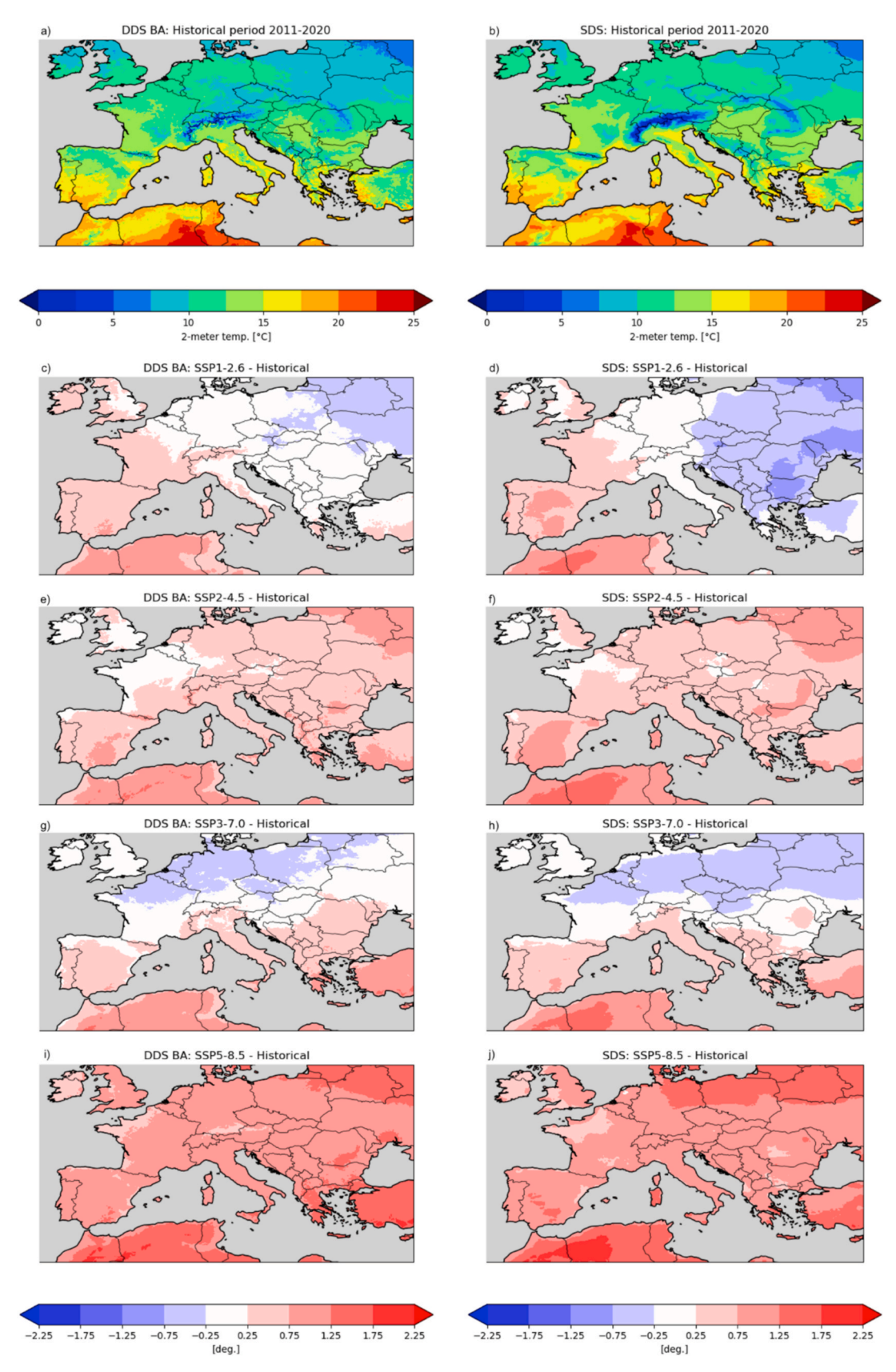
Fig. 8. Climate projections of mean precipitation obtained from DDS BA (left column) and SDS (right column) methods for the historical period (2011–2020, top row) and for the differences between each SSP (2041–2050) and the historical period means (from the second to the fifth row: SSP1-2.6, SSP2-4.5, SSP3-7.0 and SSP5-8.5).

is visible especially under the SSP3-7.0 scenario, showing a peak of warming in the 2031–2040 decade. Spring and Autumn are the seasons that less warming (only + 2°C) will experience in the region under the SSP2-4.5 and SSP3-7.0 scenarios, as these projections also show more expected precipitation (between + 10 and + 20 %) in CMTo for the following decades (not shown). The increase of moisture during Spring and Autumn is also related to the increase of temperature in the

Mediterranean seas, which is expected to produce deeper convective systems with increase of the precipitation concentration (Monjo et al., 2016, Monjo et al., 2023).

4.3. Uncertainty analysis

The annual mean precipitation bias from the raw outputs of EC-



 $\textbf{Fig. 9.} \ \ \textbf{The same as Fig. 8 but for mean temperature.}$

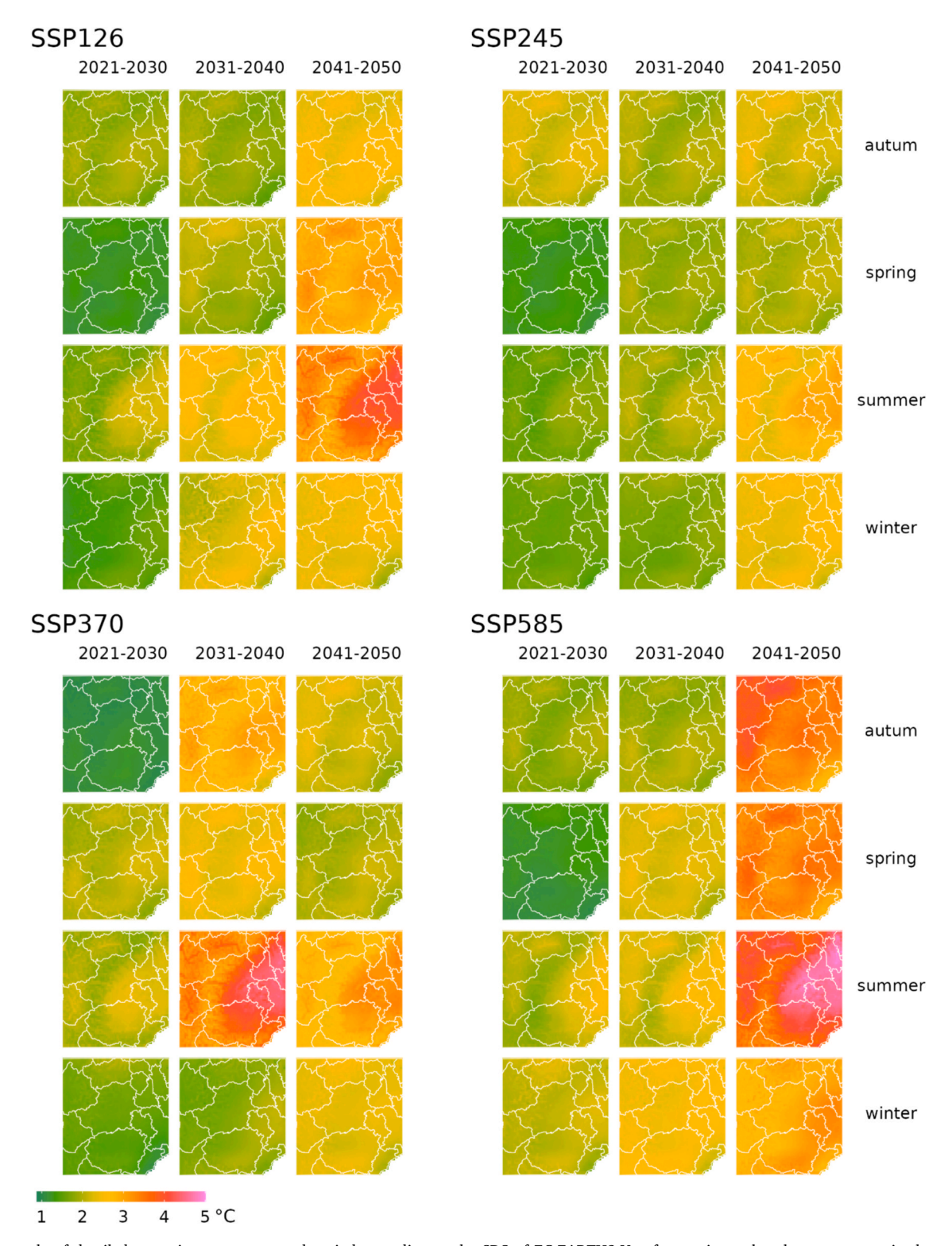


Fig. 10. Example of detailed scenarios per season and period according to the SDS of EC-EARTH3-Veg for maximum hourly temperature in the study area of Metropolitan City of Turin (CMTo) at a 3 km spatial resolution (D1 domain area, Table A1).

EARTH3-Veg brings about the added values of dynamical downscaling in representing spatial variability. An overall reduction in wet bias in the northern parts of the domain was found for DDS compared to EC-EARTH3-Veg. Also, the precipitation enhancement in orographic regions of central Europe in downscaled simulation improved the dry bias present in driving ESM.

The discrepancy underlines the limitations of each approach: DDS might overemphasize physical processes not well-represented at higher

resolutions, while SDS risks missing critical dynamical feedbacks, potentially affecting model accuracy in regions characterized by complex topography or local climatic interactions. For instance, SDS might not adequately reflect localized drought intensification seen in observational records, suggesting that neither method fully captures the region's climatic complexity. These differences highlight critical implications for impact studies. Consensual results from both methods is especially crucial for water resource management in the Mediterranean

basin, since a method's mixed over- and underestimations could lead to greater uncertainty in hydrological planning.

Concerning temperature simulations, differences between both methods are accentuated in the most mountainous regions of Central Europe but also in some litoral areas of Southeastern Europe. These differences are due to the ability of the methods to capture to a greater or lesser extent the characteristics or effects on the temperature variability from the elevation or the distance to the sea. For instance, SDS incorporates a digital elevation model and a field of distance to the see as two direct predictors during the bias correction procedure, allowing us to reduce the impact of the systematic error in the most geographically complex regions.

Therefore, our results provide insights into the strengths of combining statistically and dynamically downscaled simulations and pave the way for bias-adjustment before using local-scale climate scenarios for DISTENDER case studies. The detailed biases and projections underline the importance of using complementary methods to provide a more comprehensive picture of potential climate impacts. By comparing the strengths and limitations of DDS and SDS, stakeholders can better assess risks and uncertainties associated with future climate scenarios.

5. Conclusions

The DISTENDER project demonstrates the feasibility and benefits of integrating cutting-edge statistical and dynamical downscaling methods to address the limitations of Earth System Models (ESMs) in producing localized climate projections. By employing a novel three-stage statistical downscaling process, the project developed hourly climate scenarios that provide high temporal and spatial resolution. This innovation ensures compatibility with observed reference data, improves the representation of probability distribution tails (e.g., extreme values), and captures microclimatic features that are critical for understanding local climate risks. For instance, hourly scaling based on analogies and geostatistical adjustments allows the fine-tuning of climate projections to a resolution of $<10~\rm km$ across Europe, enabling enhanced applicability for urban and regional planning.

The SDS approach showcased strengths in computational efficiency, enabling the downscaling of multiple ESMs and emission scenarios to quantify uncertainties systematically. However, it also highlighted persistent challenges, such as biases in precipitation and temperature across regions and seasons. For example, according to the median simulation (EC-EARTH3-Veg), negative precipitation biases of up to $-1\,$ mm/day in summer were noted in southern Europe, while temperature biases ranged from $-2^{\circ}\mathrm{C}$ in Northeast Europe to $+1^{\circ}\mathrm{C}$ in central regions during winter. Despite these biases, the Kolmogorov-Smirnov (KS) tests confirmed the statistical consistency of daily precipitation and temperature distributions for most models and seasons (with p-value >0.05).

DDS, performed with the ICON model, offered additional insights into the spatial and seasonal variability of climate projections. By leveraging high-resolution domains (e.g., 3 km for core case studies), it successfully improved the representation of complex atmospheric processes, particularly over orographic regions. This method mitigated some of the statistical method's limitations, such as spatial inconsistencies and dependency on historical relationships. The reduction of wet biases in northern Europe and the enhanced depiction of summer dry periods in central Europe highlight the added value of dynamical approaches, albeit at higher computational costs.

Projections of future climate scenarios under various socioeconomic pathways revealed significant potential impacts on precipitation and temperature patterns across Europe. For instance, under SSP5-8.5, summer precipitation is projected to decrease by up to $-20\ \%$ in southern Europe, while central and northern regions may experience increases of + 10 % to + 15 %. Temperature projections indicate

pronounced warming of up to $+\,5^{\circ}\text{C}$ during summer in southern Europe, with smaller increases of $+\,2^{\circ}\text{C}$ to $+\,3^{\circ}\text{C}$ in northern areas. These projections provide critical insights for assessing climate hazards, such as heatwaves, droughts, and increased flood potential, and for developing targeted adaptation measures.

The performance of both DDS and SDS are adequate, showing consistent projections under different SSP scenarios. When possible, the combination of DDS and SDS is desired to measure the impact (systematic errors) from the statistical method choice, although SDS allows the production of a large number of ESM simulations due to its higher performance in computational cost efficiency. Moreover, it is the first time that an European project generates a high temporal (hourly) resolution-ensemble, very appropriate for feeding impact models. That is, the consistency and reliability of DISTENDER's scenarios make them valuable tools for climate impact assessments and policy planning, deriving possible adaptation measures. Their usability extends beyond the project's scope, supporting stakeholders in sectors like agriculture, water management, urban planning, and disaster risk reduction. The availability of high-resolution hourly data is particularly relevant for short-term operational planning and long-term strategic initiatives. Additionally, the dataset offers opportunities for interdisciplinary research, enabling integration with socio-economic and ecological models to evaluate broader climate impacts.

In summary, the DISTENDER project underscores the importance of leveraging both SDS and DDS approaches to achieve comprehensive and actionable climate projections. While statistical methods offer computational efficiency and extensive ensemble outputs, dynamical approaches provide the spatial and physical accuracy needed for regional applications. The combined methodology represents a significant advancement in climate modeling, paving the way for more precise, localized, and user-focused climate scenarios. Future work should focus on refining bias correction techniques, further exploring the integration of these approaches, and addressing emerging challenges such as non-stationarity and extreme event simulation, at the same time that optimizes accuracy and computational efficiency.

CRediT authorship contribution statement

Robert Monjo: Writing – original draft, Visualization, Validation, Supervision, Methodology, Investigation, Formal analysis, Conceptualization. Yassmin H. Essa: Writing – review & editing, Validation, Software, Methodology, Investigation, Formal analysis, Data curation, Conceptualization. Carlos Prado-López: Software, Data curation. Manpreet Kaur: Validation, Investigation, Conceptualization. Darío Redolat: Visualization, Validation, Investigation. César Paradinas: Writing – review & editing, Visualization, Validation, Data curation. Dominic Royé: Visualization, Validation, Supervision, Software, Resources, Formal analysis, Data curation. Bodo Ahrens: Writing – review & editing, Validation, Supervision, Methodology, Conceptualization. Roberto San José: Validation, Supervision, Project administration, Funding acquisition.

Declaration of competing interest

The authors declare the following financial interests/personal relationships which may be considered as potential competing interests: Robert Monjo reports financial support was provided by Foundation for Climate Research. Roberto San Jose reports financial support was provided by Polytechnic University of Madrid. If there are other authors, they declare that they have no known competing financial interests or personal relationships that could have appeared to influence the work reported in this paper.

Appendix A:. Description of the DISTENDER climate data

This appendix describes the characteristics of the climate data generated in DISTENDER. Table A1 shows details of the 14 domains defined in DISTENDER to model climate variables in the five Core Case Studies, with 11 domain areas at hourly scales and three at a daily scale. Table A2 details the total dataset produced at hourly scale, consisting of 19 variables (in five levels) per three CMIP6 models with five simulations (historical + four SSP projections) with 34 or 36 years per each one. Similarly, Table 3 described the data produced for the three domains considered for daily scales.

Table A1

Core Case Study domains in the DISTENDER project. The five Core Case Studies are: (1) Guimaraes; (2) The Metropolitan City of Turin (CMTo: Città Metropolitana di Torino); (3) the Hanze University of Applied Sciences (HUAS) that represents the North-east of the Netherlands; (4) the European Agroforestry Federation (Euraf) that represents Dehesas (Spain) and Montados (Portugal) areas and (5) Austria.

Core Case Study	Domain area	Time resol.	Official Lon range	Official Lat range	Produced Lon range	Produced Lat range	Resol.	Mean resolution (approx) (km)	Zonal resolution (longitude km)	Meridional resolution (latitude km)	Nlon	Nlat	Ncells	
Guimaraes	D0	hourly	-8.666;	41.183;	-8.710;	41.120;	0.09	9	7.5	9.9	11	7	77	
			-7.765	41;701	-7.72	41.750								
	D1	hourly	-8.666;	41.183;	-8.670;	41.172;	0.01	1	0.8	1.1	91	54	4914	
			-7.765	41;701	-7.76	41.713								
	D2	hourly	-8.462;	41.349;	-8.466;	41.343;	0.005	0.5	0.4	0.6	68	51	3468	
			-8.130	41.592	-8.126	41.598								
	D3	hourly	-8.373;	41.415;	-8.374;	41.414;	0.001	0.1	0.1	0.1	119	49	5831	
			-8.256	41.462	-8.255	41.463								
СМТо	D0	hourly	6.371;	44.121;	6.340;	44.060;	0.09	9	7.5	9.9	27	22	594	
			8.745	45.997	8.770	46.040								
	D1	hourly	6.371;	44.121;	6.350;	44.099;	0.03	3	2.5	3.3	80	64	5120	
			8.745	45.997	8.750	46.019								
	D2	hourly	6.500;	44.670;	6.490;	44.660;	0.01	1	0.8	1.1	172	100	17,200	
			8.200	45.650	8.210	45.660								
	D3	hourly	7.366;	44.835;	7.361;	44.829;	0.005	0.005 0.5	0.5 0.4	0.4 0.6	0.6	131	94	12,314
			8.011	45.293	8.016	45.299		_						
HUAS	D0	hourly	3.995;	51.535;	3.937;	51.47;	0.09	9	7.5	9.9	44	28	1232	
			7.839	53.932	7.890	53.9935								
	D1	hourly	4.169;	52.072;	4.153;	52.056;	0.03	3	2.5	3.3	109	63	6867	
	DO	1 1	7.408	53.932	7.423	53.946	0.01	1	0.0	1.1	107	00	16.456	
	D2	hourly	5.396;	52.609;	5.385;	52.597;	0.01	1	0.8	1.1	187	88	16,456	
F	D1	D-!1	7.245	53.465	7.255	53.477	0.00	0	7.5	9.9	100	4.4	4400	
Euraf	D1	Daily	-9.846;	37.830;	-9.888;	37.783;	0.09	9	7.5	9.9	102	44	4488	
	D2	Daile	-0.750	41.698	-0.708	41.743	0.00	0	7.5	0.0	70	25	2555	
	D2	Daily	-9.846;	37.830;	-9.883;	37.788;	0.09	9	7.5	9.9	73	35	2555	
A atui a	D1	Deiler	-3.350 9.271;	40.896	-3.313 9.230;	40.938	0.09	9	7.5	9.9	90	41	3690	
Austria	זע	Daily	,	46.019;		45.96;	0.09	9	7.5	9.9	90	41	3090	
			17.290	49.592	17.330	49.65								

Table A2
Hourly climate variables (19) simulated in 5 levels [surface (sfc), 2 m, 10 m, 50 m and 200 m] by statistical downscaling in the DISTENDER project year-by-year for the 1981–2014 and 2015–2050 periods under the Historical experiment and four SSP scenarios (SSP1-2.6, SSP2-4.5, SSP3-7.0 and SSP5-8.5). All the variables of the same level are gathered in a unique file per year of simulation.

Level	Variable	Short name	Long name	Units	Scale factor
sfc	rad	Total radiation	Hourly accumulated downward total radiation at surface	J/m ²	3600
	short_rad	Shortwave radiation	Hourly accumulated downward shortwave radiation at surface	J/m^2	3600
	long_rad	Longwave radiation	Hourly accumulated downward longwave radiation at surface	J/m^2	3600
	prec	Precipitation	Hourly cumulative precipitation	mm	0.1
2 m	temp	Temperature	Hourly average air temperature	°C	0.1
	rel_hum	Relative humidity	Hourly average air relative humidity	°C	0.1
	press	Pressure	Hourly average of air pressure given at local elevation	hPa	0.1
10 m	u-wind	u-component wind	Hourly average of eastward wind	m/s	0.1
	v-wind	v-component wind	Hourly average of northward wind	m/s	0.1
50 m & 2000 m	temp	Temperature	Hourly average air temperature	°C	0.1
	relhum	Relative humidity	Hourly average air relative humidity	%	0.1
	press	Pressure	Hourly average of air pressure given at local elevation	hPa	0.1
	u-wind	u-component wind	Hourly average of eastward wind	m/s	0.1
	v-wind	v-component wind	Hourly average of northward wind	m/s	0.1

Table A3

Daily climate variables (33) simulated in 5 levels (sfc, 2 m, 10 m, 50 m and 200 m) by statistical downscaling in the DISTENDER project year-by-year for the 1981–2014 and 2015–2050 periods under the Historical experiment and four SSP scenarios (SSP1-2.6, SSP2-4.5, SSP3-7.0 and SSP5-8.5). All the variables of the same level are gathered in a unique file per year of simulation.

Level	Variable	Short name	Long name	Units	Scale factor
sfc	rad	Total radiation	Mean power of downward total radiation at surface in a day	W/m ²	1
	short_rad	Shortwave radiation	Mean power of downward shortwave radiation at surface in a day	W/m^2	1
	long_rad	Longwave radiation	Mean power of downward longwave radiation at surface in a day	W/m^2	1
	prec	Precipitation	Total accumulate precipitation in a day	mm	0.1
2 m	temp_mean	Mean temperature	Mean air temperature of a day	°C	0.1
	temp_min	Minimum temperature	Minimum air temperature of a day	°C	0.1
	temp_max	Maximum temperature	Maximum air temperature of a day	°C	0.1
	relhum_mean	Mean relative humidity	Mean air relative humidity of a day	%	0.1
	relhum_min	Minimum relative humidity	Minimum air relative humidity of a day	%	0.1
	relhum_max	Maximum relative humidity	Maximum air relative humidity of a day	%	0.1
	press	Pressure	Average of air pressure given at local elevation in a day	hPa	0.1
10 m	u-wind_mean	Mean u-component wind	Average of eastward wind in a day	m/s	0.1
	v-wind_mean	v-component wind	Average of northward wind in a day	m/s	0.1
50 m & 2000 m	temp_mean	Mean temperature	Mean air temperature of a day	°C	0.1
	temp_min	Minimum temperature	Minimum air temperature of a day	$^{\circ}\mathrm{C}$	0.1
	temp_max	Maximum temperature	Maximum air temperature of a day	$^{\circ}\mathrm{C}$	0.1
	relhum_mean	Mean relative humidity	Mean air relative humidity of a day	%	0.1
	relhum_min	Minimum relative humidity	Minimum air relative humidity of a day	%	0.1
	relhum_max	Maximum relative humidity	Maximum air relative humidity of a day	%	0.1
	press	Pressure	Average of air pressure given at local elevation in a day	hPa	0.1
	u-wind_mean	Mean u-component wind	Average of eastward wind in a day	m/s	0.1
	v-wind_mean	v-component wind	Average of northward wind in a day	m/s	0.1
	temp_mean	Mean temperature	Mean air temperature of a day	°C	0.1

Data availability

Data will be made available on request.

References

- Ban, N., Brisson, E., Ahrens, B., Caillaud, C., Coppola, E., Pichelli, E., Sobolowski, S., Adinolfi, M., et al., 2021. The first multi-model ensemble of regional climate simulations at kilometer-scale resolution, Part I: evaluation of precipitation. Climate Dynamics. https://doi.org/10.1007/s00382-021-05708-w.
- Benestad, R.E., 2010. Theor. Appl. Climatol. 100, 1–21. https://doi.org/10.1007/s00704-009-0158-1.
- Brun, P., Zimmermann, N.E., Hari, C., Pellissier, L., Karger, D.N., 2022. Global climate-related predictors at kilometre resolution for the past and future. Earth Syst. Sci. Data Discuss. https://doi.org/10.5194/essd-2022-212 [preprint].
- Copernicus-C3S, 2020. High-resolution climate projections. Climate Data Factory. https://climate.copernicus.eu/high-resolution-climate-projections.
- Copernicus-C3S, 2022. Climadjust, a Bias-Adjustment service for the Climate Data Store. https://climate.copernicus.eu/climadjust-bias-adjustment-service-climate-data-store.
- Copernicus-C3S, 2024. ERA5-Land hourly data from 1950 to present. Climate Change Service: DOI: 10.24381/cds.adbb2d47. Link with dataset metadata: https://cds.climate.copernicus.eu/datasets/reanalysis-era5-land?tab=overview.
- Cornes, R., van der Schrier, G., van den Besselaar, E.J.M., Jones, P., 2018. An ensemble version of the E-OBS Temperature and precipitation datasets. J. Geophys. Res. Atmos. 123.
- Cos, J., Doblas-Reyes, F., Jury, M., Marcos, R., Bretonnière, P.-A., Samsó, M., 2022. The Mediterranean climate change hotspot in the CMIP5 and CMIP6 projections. Earth Syst. Dyn. 13, 321–340. https://doi.org/10.5194/esd-13-321-2022.
- Dobler, A., Ahrens, B., 2008. Precipitation by a regional climate model and bias correction in Europe and South Asia. Meteorol. Z. 17, 499–509. https://doi.org/ 10.1127/0941-2948/2008/0306.
- Döscher, R., Acosta, M., Alessandri, A., Anthoni, P., Arsouze, T., Bergman, T., Bernardello, R., Boussetta, S., Caron, L.-P., Carver, G., Castrillo, M., Catalano, F., Cvijanovic, I., Davini, P., Dekker, E., Doblas-Reyes, F.J., Docquier, D., Echevarria, P., Fladrich, U., Fuentes-Franco, R., Gröger, M., 2022. The EC-EARTH-3Veg Earth system model for the coupled Model Intercomparison Project 6. Geosci. Model Dev. 15, 2973–3020. https://doi.org/10.5194/gmd-15-2973-2022.
- Dyrrdal, A.V., Stordal, F., Lussana, C., 2018. Evaluation of summer precipitation from EURO-CORDEX fine-scale RCM simulations over Norway. Int. J. Climatol. 38 (4), 1661–1677.
- EEA, 2020. Corine-2018: Corine Land Cover 2018 (raster 100 m), Europe, 6-yearly version 2020_20u1, May 2020. Copernicus Land Monitoring Service, European Environment Agency (EEA). DOI: 10.2909/960998c1-1870-4e82-8051-6485205ebbac Retrieved from https://www.eea.europa.eu/data-and-maps/data/external/corine-land-cover-2018.

- Eyring, V., Bony, S., Meehl, G.A., Senior, C.A., Stevens, B., Stouffer, R.J., Taylor, K.E., 2016. Overview of the coupled Model Intercomparison Project phase 6 (CMIP6) experimental design and organization. Geosci. Model Dev. 9, 1937–1958. https://doi.org/10.5194/gmd-9-1937-2016.
- Gutiérrez, J.M., et al., 2018. An intercomparison of a large ensemble of statistical downscaling methods over Europe: results from the VALUE perfect predictor cross-validation experiment. Int. J. Climatol. 2018, 1–36. https://doi.org/10.1002/ioc.5462
- Hersbach, H., Bell, B., Berrisford, P., et al., 2020. The ERA5 global reanalysis. Q. J. R. Meteorol. Soc. 146, 1999–2049. https://doi.org/10.1002/qj.3803.
- Hetzer, J., Forrest, M., Ribalaygua, J., Prado-López, C., Hickler, T., 2024. The fire weather in Europe: large-scale trends towards higher danger. Environ. Res. Lett. 19 (8), 084017. https://doi.org/10.1088/1748-9326/ad5b09 1.
- IPCC, 2021. Climate Change 2021: The Physical Science Basis. Contribution of Working Group I to the Sixth Assessment Report of the Intergovernmental Panel on Climate Change. Cambridge University Press, Cambridge, United Kingdom and New York, NY, USA, In press, doi:10.1017/9781009157896.
- Monjo, R., Caselles, V., Chust, G., 2014. Probabilistic correction of RCM precipitation in the Basque Country (Northern Spain). Theor. Appl. Climatol. 117, 317–329. https://doi.org/10.1007/s00704-013-1008-8.
- Monjo, R., Gaitán, E., Pórtoles, J., Ribalaygua, J., Torres, L., 2016. Changes in extreme precipitation over Spain using statistical downscaling of CMIP5 projections. Int. J. Climatol. 36, 757–769. https://doi.org/10.1002/joc.4380.
- Monjo R, Prado C, Redolat D, Gaitán E, Paradinas C, Rubio T, Torres, L., 2021. Climate Risk Information for SupportIng ADAptation Planning and operaTion (CRISI-ADAPT II): CMIP5-CMIP6 comparison. 8th International Conference on Meteorology and climatology of the Mediterranean (MetMed), 26-27 May 2021.
- Monjo, R., Locatelli, L., Milligan, J., Torres, L., Velasco, M., Gaitán, E., Pórtoles, J., Redolat, D., Russo, B., Ribalaygua, J., 2023. Estimation of future extreme rainfall in Barcelona (Spain) under monofractal hypothesis. Int. J. Climatol. https://doi.org/10.1002/joc.8072.
- Prill, F., Reinert, D., Rieger, D., Zängl, G., 2022. Working with the ICON Model. Deutscher Wetterdienst, Offenbach, Hessen (Germany). doi:10.5676/DWD_pub/nwv/icon tutorial2020.
- Relvas, H., Monjo, R., Coelho, S., et al., 2025. Rising Temperatures, Rising Risks: Heat-Related Mortality in Europe Under Climate Change. Earth Syst Environ. DOI: 10.1007/s41748-025-00692-1.
- Ribalaygua, J., Torres, L., Pórtoles, J., Monjo, R., Gaitán, E., Pino, M.R., 2013.
 Description and validation of a two-step analogue/regression downscaling method.
 Theor. Appl. Climatol. 114, 253–269. https://doi.org/10.1007/s00704-013-0836-x.
- Ridal, M., Bazile, E., Le Moigne, P., Randriamampianina, R., Schimanke, S., Andrae, U., et al., 2024. CERRA, the Copernicus European regional reanalysis system. Q. J. R. Meteorolog. Soc. 150 (763), 3385–3411. https://doi.org/10.1002/qj.4764.
- San Jose, R., Perez-Camanyo, J.L., Jiménez Gañan, M., 2024. Impacts on biogenic carbon dioxide emission fluxes driven by generated numerical-downscaled climate scenarios. Eur. J. Sustain. Develop. 13 (4), 467–476. https://doi.org/10.14207/ ejsd.2024.v13n4p467.
- Seaby L.P., Refsgaard J.C., Sonnenborg T.O., Stisen S., Christensen J.H., Jensen K.H., 2013. Assessment of robustness and significance of climate change signals for an

- ensemble of distribution-based scaled climate projections, J. Hydrol., 486, 479-493, ISSN 0022-1694, doi:10.1016/j.jhydrol.2013.02.015.
- Sekhon, J.S., 2010. Matching: Multivariate and Propensity Score Matching with Balance Optimization. R package version 4.7-11. URL http://CRAN.Rproject.org/ package=Matching.
- Schmidli, J., Frei, C., Vidale, P.L., 2006. Downscaling from GCM precipitation: a benchmark for dynamical and statistical downscaling methods. Int. J. Climatol. 26, 679–689. https://doi.org/10.1002/joc.1287.
- Somot, S., Ruti, P., Ahrens, B., Coppola, E., Jordà, G., Sannino, G., Solmon, F., 2018. Editorial for the Med-CORDEX special issue. Clim. Dyn. 51, 771. https://doi.org/ 10.1007/s00382-018-4325-x.
- Swart, N.C., Cole, J.N.S., Kharin, V.V., Lazare, M., Scinocca, J.F., Gillett, N.P., Anstey, J., Arora, V., Christian, J.R., Hanna, S., Jiao, Y., Lee, W.G., Majaess, F., Saenko, O.A., Seiler, C., Seinen, C., Shao, A., Sigmond, M., Solheim, L., von Salzen, K., Yang, D., Winter, B., 2019. The Canadian earth system model version 5 (CanESM5.0.3). Geosci. Model Dev. 12, 4823–4873. https://doi.org/10.5194/gmd-12-4823-2019.
- Tang, J., Niu, X., Wang, S., Gao, H., Wang, X., Wu, J., 2016. Statistical downscaling and dynamical downscaling of regional climate in China: present climate evaluations and

- future climate projections. J. Geophys. Res. Atmos. 121, 2110–2129. https://doi.org/10.1002/2015JD023977.
- Torres L, Monjo R, Prado C, Pórtoles J, Muñoz A, Gaitán E., Redolat D., Paradinas C., de Juan, M., Ribalaygua J., 2020. Comparativa de simulaciones de clima futuro local en entornos marítimoportuarios. sinergias entre los proyectos ECCLIPSE y CRISI-ADAPT II. Uhinak, IV Congreso transfronterizo sobre cambio climático y litoral, 4-5 Novembere 2020, Irun.
- Trzaska, S., Schnarr, E., 2014. A Review of Downscaling Methods for Climate Change Projections.
- Venables, W.N., Ripley, B.D., 2002. Modern Applied Statistics with S, (4th ed). Springer, New York
- Von Storch, J.-S., Putrasahan, D., Lohmann, K., et al., 2017. MPI-M MPIESM1.2-HR model output prepared for CMIP6 HighResMIP. Earth System Grid Federation. https://doi.org/10.22033/ESGF/CMIP6.762.
- Wouters, H., Varentsov, M., Blahak, U., Schulz, J.-P., Schättler, U., Bucchignani, E., Demuzere, M., 2017. User guide for TERRA URB v2.2: The urban-canopy landsurface scheme of the COSMO model. 10.13140/RG.2.2.33691.87847/1.